Chapter 5
Cuspless Sub-Riemannian Geodesics within the Euclidean Motion Group $SE(d)$

Remco Duits, Arpan Ghosh, Tom Dela Haije, and Yuri Sachkov

Abstract. We consider the problem $\mathbf{P}_{curve}$ of minimizing $\int_0^\ell \sqrt{\beta^2 + |\kappa(s)|^2}\mathrm{d}s$ for a planar curve having fixed initial and final positions and directions. Here κ is the curvature of the curve with free total length ℓ. This problem comes from a 2D model of geometry of vision due to Petitot, Citti and Sarti. Here we will provide a general theory on cuspless sub-Riemannian geodesics within a sub-Riemannian manifold in $SE(d)$, with $d \geq 2$, where we solve for their momentum in the general d-dimensional case. We will explicitly solve the curve optimization problem $\mathbf{P}_{\mathbf{curve}}$ in 2D (i.e. $d = 2$) with a corresponding cuspless sub-Riemannian geodesic lifted problem defined on a sub-Riemannian manifold within $SE(2)$. We also derive the solutions of $\mathbf{P}_{\mathbf{curve}}$ in 3D (i.e. $d = 3$) with a corresponding cuspless sub-Riemannian geodesic problem defined on a sub-Riemannian manifold within $SE(3)$. Besides exact formulas for cuspless sub-Riemannian geodesics, we derive their geometric properties, and we provide a full analysis of the range of admissible end-conditions. Furthermore, we apply this analysis to the modeling of association fields in neurophysiology.

5.1 Introduction

Curve optimization plays a major role both in imaging and visual perception. In imaging there exist many works on snakes and active contour modeling, whereas in visual perception illusionary contours arise in various optical illusions [38, 42]. Mostly, such snake and active contour models involve curve optimization in $\mathbb{R}^d$,

Remco Duits · Arpan Ghosh · Tom Dela Haije
IST/e, Eindhoven University of Technology, IST/e, Den Dolech 2,
NL-5600 MB, The Netherlands
e-mail: {R.Duits,A.Ghosh,T.C.J.Dela.Haije}@tue.nl

Yuri Sachkov
Program Systems Institute, Russian Academy of Sciences
e-mail: sachkov@sys.botik.ru

G. Citti and A. Sarti (eds.), *Neuromathematics of Vision,*
Lecture Notes in Morphogenesis,
DOI: 10.1007/978-3-642-34444-2_5, © Springer-Verlag Berlin Heidelberg 2014

$d \geq 2$, that rely on Euler's elastica curves [24] (minimizing $\int (|\kappa|^2 + \beta^2) \mathrm{d}s$) in order to obtain extensions where typically external forces to the data are included, cf. [9, 12, 50–52] .

The elastica problem suffers from the well-known fact that not every stationary curve is a global minimizer, e.g. many local minimizers exist, cf. Figure 5.1. Stationarity of a curve can be reasonably checked by the visual system using local perturbations, whereas checking for (global) optimality [45, 46] is much more difficult. Some visual illusions (e.g. the Kanisza triangle) involve corners requiring abrupt resetting of initial and ending conditions, which are difficult to explain in the elastica model. Another problem with elastica is that it is very hard to solve the boundary value problem analytically [3, 4], and typically require $(2d-1)$-dim. shooting schemes. On top of that elastica curves relate to modes of the direction process (for contour-completion [21, 23, 38, 50]) where the direction of an oriented random walker is deterministic and its orientation is random. Such deterministic propagation only makes sense when the initial orientation is sharply defined. Instead Brownian motion with random behavior both in spatial propagation direction and in orientation direction ([2, 13, 19, 22]), relates to hypo-elliptic diffusion on the planar roto-translation group. Such a Brownian motion models contour enhancement [19] rather than contour completion [21], see [17] for a short overview. The corresponding Brownian bridge measures [22, 57] (relating to so-called completion fields in imaging [3, 21, 53]) tend to concentrate towards optimal sub-Riemannian geodesics [7, 13, 20, 35, 37, 45]. So both elastica curves and sub-Riemannian geodesics relate to two different fundamental left-invariant stochastic processes on sub-Riemannian manifolds on the 2D-Euclidean motion group [21] (respectively to the direction process and to hypo-elliptic Brownian motion).

In short, advantages of the sub-Riemannian geodesic model over the elastica model are:

- If $d = 2$, every cuspless sub-Riemannian geodesic is a global minimizer [8, 15].
- The Euler-Lagrange ODE for momentum (including normalized curvature vector $\underline{\kappa}/\sqrt{|\underline{\kappa}|^2 + \beta^2}$) can be reduced to a linear one,
- The boundary value problem can be tackled via effective analytic techniques,
- If $d = 2$, the locations where global optimality is lost can be derived explicitly.
- Sub-Riemannian geodesics (in contrast to lifted elastica) are parametrization independent in the roto-translation group $SE(d)$. Here we note in case $d = 2$, the sub-Riemannian manifold $(SE(2), \Delta_2, G_\beta)$ is encoded via a pinwheel structure of cortical columns in the primary visual cortex [41].

However, the practical drawback of sub-Riemannian geodesics compared to elastica is that their spatial projections may exhibit cusps and it is hard to analyze when such a cusp occurs. Therefore, in this article we provide a complete analysis of such sub-Riemannian geodesics, their parametrization, solving the boundary value problem, and we show precisely when a cusp occurs. See Figure 5.3 and see Figure 5.2.

A variant of the sub-Riemannian problem that ensures avoiding cusps is the following variational problem, which we will explain next.

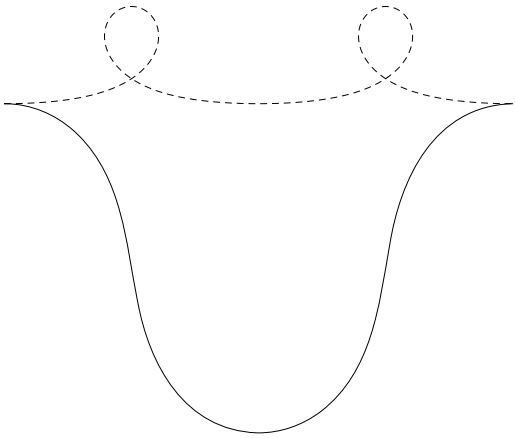

Fig. 5.1 Stationary curves of the elastica problem ($\int_0^\ell \kappa^2(s) + \beta^2 \mathrm{d}s \to \min$) do not need to be global minimizers, cf. [44]. E.g. the non-dashed elastica is a global minimum (for $\beta = 1$), whereas in dashed lines we have depicted a local minimum. This is in contrast to cuspless sub-Riemannian geodesics in $(SE(2), \Delta_2, G_\beta)$ where every stationary curve is globally optimal.

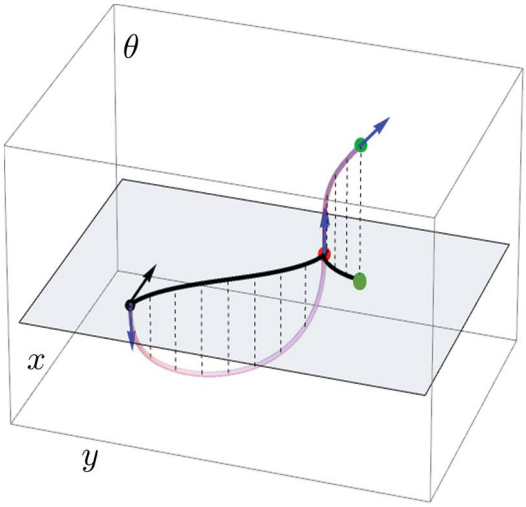

Fig. 5.2 An example of a smooth sub-Riemannian geodesic in $(SE(2), \Delta_2, G_\beta)$ whose spatial projection shows a cusp

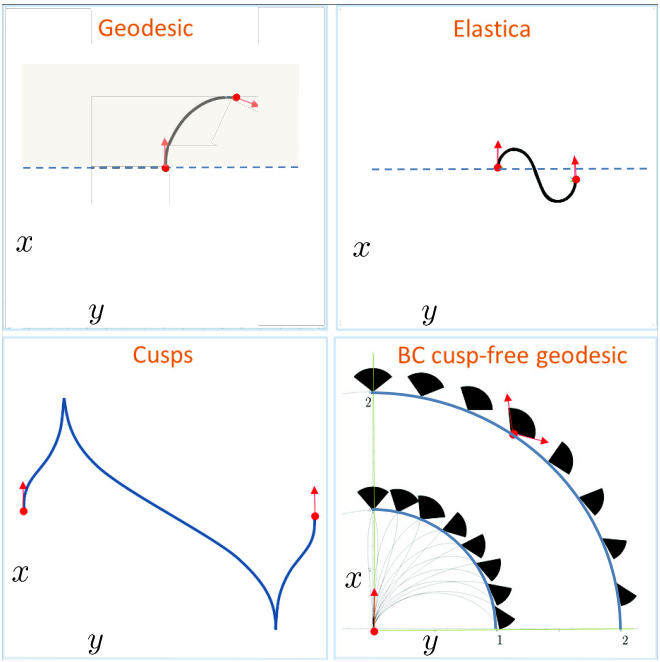

Fig. 5.3 Top left: example of a spatially projected sub-Riemannian geodesic without cusp (i.e. a solution of $\mathbf{P}_{\mathbf{curve}}$). Top right: example of an elastica curve reaching points $x < 0$. Such a (weak) connection is not possible with cuspless sub-Riemannian geodesics. Instead we see in the bottom left figure a comparable example of a spatially projected sub-Riemannian geodesic connecting the $g_{in} = (0,0,0)$ with $g_{fin} = (0, y_{fin}, 0)$ via two cusps. Bottom right: not all points in $x \geq 0$ can be reached via a globally minimizing geodesic, here we have depicted the set $\mathfrak{R}$ of admissible end-conditions $g_{fin} = (x_{fin}, y_{fin}, \theta_{fin})$ via black cones on half circles with radius 1 and 2.

On the space of sufficiently regular curves in $\mathbb{R}^d$, we define a functional $\mathscr{E} : W^{2,1}([0,\ell],\mathbb{R}^d) \to \mathbb{R}^+$, with $\ell \in \mathbb{R}^+$ being the length (free) of the curves, by

$$\mathscr{E}(\mathbf{x}) := \int_0^\ell \sqrt{\kappa(s)^2 + \beta^2}\, \mathrm{d}s. \tag{5.1}$$

Here, s denotes the arc-length parameter of curve $\mathbf{x}$ and $\kappa : [0,\ell] \to \mathbb{R}^+ \cup \{\infty\}$ denotes the absolute curvature $\|\ddot{\mathbf{x}}(\cdot)\|$ of the curve $\mathbf{x}$ at each arc-length, and $\beta > 0$ is a constant.

The two dimensional case (i.e. $d = 2$) of this variational problem was studied as a possible model of the mechanism used by the primary visual cortex V1 of the human brain to reconstruct curves which are partially hidden or corrupted. The two dimensional model was initially due to Petitot (see [40, 41] and references therein). Subsequently, the sub-Riemannian structure was introduced in the problem by Petitot [42] for the contact geometry of the fiber bundle of the 1-jets of curves in the

plane (the polarized Heisenberg group) and by Citti and Sarti [13, 47] for the principal bundle on $SE(2)$ also considered in this article. The stationary curves of the problem were derived and studied by Boscain, Charlot and Rossi in [7], by Duits in [20], by Sachkov in [35] and their global optimality is shown by Boscain, Duits, Rossi and Sachkov in [8, 15]. The two dimensional problem relates to a mechanical problem completely solved by Sachkov [37, 45, 46]. It was also studied by Hladky and Pauls in [32] and by Ben-Yosef and Ben-Shahar in [6]. Within Section 3 of this article we will summarize only the main results from our previous works [8, 15]. For detailed proofs of these results, we refer the reader to [8, 15].

Many imaging applications such as DW-MRI require an extension to higher dimensions, see e.g. [14, 23, 27, 50], which motivates us to study the higher dimensional curve optimization of the functional given by Eq. (5.1).

Let $\mathbf{x}_0, \mathbf{x}_1 \in \mathbb{R}^d$ and $\mathbf{n}_0, \mathbf{n}_1 \in S^{d-1} = \{\mathbf{v} \in \mathbb{R}^d \,|\, \|\mathbf{v}\| = 1\}$. The goal is to find an arc-length parameterized curve $s \mapsto \mathbf{x}(s)$ such that

$$\mathbf{x} = \arg \inf_{\substack{\mathbf{y} \in W^{2,1}([0,\ell],\mathbb{R}^d),\ell, \\ \mathbf{y}(0) = \mathbf{x}_0,\ \dot{\mathbf{y}}(0) = \mathbf{n}_0, \\ \mathbf{y}(\ell) = \mathbf{x}_1,\ \dot{\mathbf{y}}(\ell) = \mathbf{n}_1}} \mathscr{E}(\mathbf{y}). \tag{5.2}$$

We shall refer to this curve optimization problem as problem **P**. We assume that the boundary conditions $(\mathbf{x}_0, \mathbf{n}_0)$ and $(\mathbf{x}_1, \mathbf{n}_1)$ are chosen such that a minimizer exists.

Remark 5.1. Due to rotation and translational invariance of the problem **P**, it is equivalent to the problem with the same functional, but with boundary conditions $(\mathbf{0}, \mathbf{a})$ and $(R_{\mathbf{n}_0}^T(\mathbf{x}_1 - \mathbf{x}_0), R^T\mathbf{n}_1)$, where $\mathbf{a} \in S^{d-1}$ is a fixed axis, and with $R_{\mathbf{n}_0}$ is any rotation that maps a fixed reference axis $\mathbf{a}$ to $\mathbf{n}_0 \in S^{d-1}$.

Remark 5.2. The physical dimension of parameter β is $[\text{Length}]^{-1}$. From a physical point of view it is crucial to make the energy integrand dimensionally consistent. However, the problem with $\beta > 0$ is equivalent up to a scaling to the problem with $\beta = 1$: The minimizer $\mathbf{x}$ of **P** with $\beta > 0$ and boundary conditions $(\mathbf{x}_1, \mathbf{n}_1)$ relates to the minimizer $\overline{\mathbf{x}}$ of **P** with $\beta = 1$ and boundary condition $(\beta\mathbf{x}_1, \mathbf{n}_1)$ by spatial re-scaling, $\mathbf{x}(s) = \beta^{-1}\overline{\mathbf{x}}(s)$.

Therefore, without loss of generality, we set (unless explicitly stated otherwise)

$$\beta = 1,\ \mathbf{x}_0 = \mathbf{0},\ \text{and}\ \mathbf{n}_0 = \mathbf{e}_d$$

for the remainder of the article. Hence, the problem now is to find a sufficiently smooth arc-length parameterized curve $s \mapsto \mathbf{x}(s)$ such that

$$\mathbf{x} = \arg \inf_{\substack{\mathbf{y} \in W^{2,1}([0,\ell],\mathbb{R}^d),\ell \geq 0, \\ \mathbf{y}(0) = \mathbf{0},\ \dot{\mathbf{y}}(0) = \mathbf{e}_d, \\ \mathbf{y}(\ell) = \mathbf{x}_1,\ \dot{\mathbf{y}}(\ell) = \mathbf{n}_1}} \mathscr{E}(\mathbf{y}). \tag{5.3}$$

We refer to the above problem as $\mathbf{P}_{\mathbf{curve}}$.

We stress that there are restrictions on the boundary conditions for problem $\mathbf{P}$ and problem $\mathbf{P}_{\mathbf{curve}}$ to be well-posed [7]. For instance in case $d = 2$, one must have

$$\left(R_{\mathbf{n}_{in}}^{-1}(\mathbf{x}_{in} - \mathbf{x}_{fin}), R_{\mathbf{n}_{in}}^{-1}\mathbf{n}_{fin}\right) \in \mathfrak{R}, \tag{5.4}$$

where in $d = 2$ we have $\mathbf{n}_{fin} = (\cos(\theta_{fin}), \sin(\theta_{fin}))^T$ and where $\mathfrak{R}$ denotes the range of the exponential map [8,15]. Roughly speaking this means that the endpoint in $\mathbf{P}_{\mathbf{curve}}$ must be chosen such that it can be connected with a stationary curve.

In the d-dimensional setting criterium (5.4) is necessary, but so far it is still an open problem whether it is sufficient (for $d > 2$). Therefore, in this article we will lift and extend problem $\mathbf{P}_{\mathbf{curve}}$ to a problem $\mathbf{P}_{\mathbf{mec}}$ of finding sub-Riemannian geodesics within $SE(d)$, which is well-posed regardless the end-condition. Then subsequently, we assume the end-condition in problem $\mathbf{P}_{\mathbf{curve}}$ is chosen such that this end-condition gives rise to sub-Riemannian geodesic without cusps (i.e. $\dot{x}(t) \neq 0$ at the interior of the curve). Criterium (5.4) is then satisfied. Before we can formally introduce this problem $\mathbf{P}_{\mathbf{mec}}$ we need some preliminaries.

5.1.1 Preliminaries and Notations

- The group of rotations in $\mathbb{R}^d$ equals $SO(d) = \{R \in \mathbb{R}^{d\times d} \,|\, R^T = R^{-1}, \det(R) = 1\}$
- The special Euclidean motion group on $\mathbb{R}^d$ is given by the semi-direct product $SE(d) = \mathbb{R}^d \rtimes SO(d)$. Its group elements are denoted by $g = (\mathbf{x}, R)$ and it is endowed with group product $(\mathbf{x}_1, R_1)(\mathbf{x}_2, R_2) = (R_1\mathbf{x}_2 + \mathbf{x}_1, R_1R_2)$. Its unity element equals $e = (\mathbf{0}, I)$ with I denoting the $d \times d$ identity matrix. The group $SE(d)$ acts on the set $\mathbb{R}^d \times S^{d-1}$ via

$$(\mathbf{x}, R)(\mathbf{y}, \mathbf{n}) = (R\mathbf{y} + \mathbf{x}, R\mathbf{n}). \tag{5.5}$$

- Let $\mathbf{a} \in S^d$ be a fixed element on the d-dimensional Euclidean sphere $S^d := \{\mathbf{x} \in \mathbb{R}^d \,|\, \|\mathbf{x}\| = 1\}$. We set $\mathbf{a} = \mathbf{e}_d$, e.g. if $d = 3$ we set $\mathbf{a} = \mathbf{e}_z := (0,0,1)^T$, if $d = 2$ we set $\mathbf{a} = \mathbf{e}_y := (0,1)^T$.
- Let $d \geq 2$. The coupled space of positions and directions is defined as the Lie group quotient

$$\mathbb{R}^d \rtimes S^{d-1} := SE(d)/(\{\mathbf{0}\} \times SO(d-1)) \tag{5.6}$$

  where we identify $SO(d-1)$ with $\{R \in SO(d) \,|\, R\mathbf{a} = \mathbf{a}\}$. For simplicity elements of $\mathbb{R}^d \rtimes S^{d-1}$ are denoted by $(\mathbf{y}, \mathbf{n})$ with $\mathbf{y} \in \mathbb{R}^d$ and $\mathbf{n} \in S^{d-1}$, where we keep in mind that each element represents a left coset within $SE(d)$. Such a left-coset contains equivalent rigid body motions that map $(\mathbf{0}, \mathbf{a})$ to $(\mathbf{y}, \mathbf{n})$ via the rigid body motion action (5.5):

$$(\mathbf{y}, \mathbf{n}) = (\mathbf{y}, R_{\mathbf{n}})(\mathbf{0}, \mathbf{a})$$

  where $R_{\mathbf{n}} \in SO(d)$ denotes *any* rotation that maps $\mathbf{a}$ onto $\mathbf{n} \in S^{d-1}$.
- The left-invariant vector fields considered as differential operators acting on smooth functions $\phi : SE(d) \to \mathbb{R}$ are given by the push-forward of the left multiplication $L_g : SE(d) \to SE(d)$ given by $L_g h = gh$:

$$\mathscr{A}_g = (L_g)_* \mathscr{A}_e, \text{ i.e. } \mathscr{A}_g \phi = \mathscr{A}_e(\phi \circ L_g), \tag{5.7}$$

where $\mathscr{A}_e \in T_e(SE(d))$, with $T_e(SE(d))$ the tangent space at the unity element e.

- We choose[1] a basis in $T_e(SE(d))$, say $\{A_1,\ldots,A_d\} \cup \{A_{d+1},\ldots,A_{d(d+1)/2}\}$ with vector fields $A_j = \frac{\partial}{\partial x^j}$, $j = 1,\ldots,d$ acting only on the spatial part[2], and $\{A_{d+1},\ldots,A_{d(d+1)/2}\}$ acting only on the $SO(d)$ part. The matrix representations of the spatial generators are given by

$$A_k = \begin{pmatrix} 0 & \mathbf{e}_k \\ 0 & 0 \end{pmatrix} \in \mathbb{R}^{(d+1)\times(d+1)}, k = 1\ldots d.$$

The matrix representations of these angular generators in $T_e(SE(d))$ are given by

$$A_{d(d+1)/2-i+1} = \begin{cases} \begin{pmatrix} -E^n_{n+1} + E^{n+1}_n & \mathbf{0} \\ 0 & 0 \end{pmatrix}, & \text{if } i = n(n+1)/2 \\ & \text{for some } n \in \{1,\ldots,d-1\}, \\ \begin{pmatrix} E^{i_0}_{n+2} - E^{n+2}_{i_0} & \mathbf{0} \\ 0 & 0 \end{pmatrix}, & \text{if } i = n(n+1)/2 + i_0 \\ & \text{with } i_0 \in \{1,\ldots,n\} \\ & \text{for some } n \in \{1,\ldots,d-1\}. \end{cases} \tag{5.8}$$

with $E^i_j \in \mathbb{R}^{d\times d}$ a matrix with all zero elements except for a unity 1 in row i and column j. In this way we have

$$\text{span}\{\mathscr{A}_{d+1},\ldots,\mathscr{A}_{d(d+1)/2}\} \equiv T_e(SO(d)) = so(d) = \text{span}\{E^i_j - E^j_i \mid 1 \le i < j \le d\}.$$

Furthermore, we observe that the angular generators are ordered such that

$$\text{span}\{A_{2d},\ldots,A_{d(d+1)/2}\} \equiv T_e(\{0\} \times SO(d-1)). \tag{5.9}$$

So in view of $\mathbb{R}^d \rtimes S^{d-1}$, Eq. (5.6), the redundant directions in $SE(d)$ (i.e. the angular generators of the stabilizing sub-group of $\mathbf{a}$, which is isomorphic to $SO(d-1)$) come at the end. To this end we note that

$$\begin{aligned} d(d+1)/2 = \dim(SE(d)) &= \dim(\mathbb{R}^d \rtimes S^{d-1}) + \dim(SO(d-1)) \\ &= (2d-1) + (d-2)(d-1)/2. \end{aligned} \tag{5.10}$$

Via the push-forward $(L_g)_*$ of the left-multiplication, Eq. (5.7), this basis $\{A_1,\ldots,A_{d(d+1)/2}\}$ provides us a moving frame of reference in the group $SE(d)$. This basis will be denoted by $\{\mathscr{A}_1,\ldots,\mathscr{A}_{d(d+1)/2}\}$ with

$$\mathscr{A}_i|_g = (L_g)_* A_i \text{ , for all } i = 1\ldots,d(d+1)/2, g \in SE(d), \tag{5.11}$$

[1] The main results (in contrast to the structure constants $c^k_{i,j}$) in this article do not depend on this choice of basis, one may choose a different basis with an ordering such that (5.9) holds.

[2] In previous works [19, 20] on $SE(2)$, different ordering conventions are used in the Lie-algebra, and we set $\mathbf{a} = \mathbf{e}_x$ instead of $\mathbf{a} = \mathbf{e}_y$. In subsections 3.2–3.5 we will also adhere to that convention.

with $A_i = \mathscr{A}_i|_{g=e}$. The corresponding dual frame $\{\omega^k\}_{k=1,\ldots,d(d+1)/2}$ is given by

$$\langle \omega^k\Big|_g, \mathscr{A}_j\big|_g\rangle = \delta^k_j, \text{ for all } k,j = 1,\ldots,d(d+1)/2 \text{ and all } g \in SE(d), \quad (5.12)$$

where δ^i_j are the usual components of the Kronecker tensor. Explicit formulas for the frame of left-invariant vector fields and corresponding dual frame are derived in [18, 20]. Note that the vector space of left-invariant vector fields forms a Lie-algebra, with structure constants $c^k_{i,j}$ given by

$$[\mathscr{A}_i, \mathscr{A}_j] = \mathscr{A}_i\mathscr{A}_j - \mathscr{A}_j\mathscr{A}_i = \sum_{k=1}^{d(d+1)/2} c^k_{i,j}\mathscr{A}_k. \quad (5.13)$$

- Within this article we consider the sub-Riemannian manifold $(SE(d), \Delta_d, G_\beta)$, with base manifold $SE(d)$, and with distribution Δ_d, and metric tensor $G_\beta : SE(d) \times \Delta_d \times \Delta_d \to \mathbb{R}$ given by

$$\begin{aligned} &\Delta_d = \text{span}\{\mathscr{A}_d, \ldots, \mathscr{A}_{2d-1}\}, \\ &G_\beta\big|_g \left(\sum_{i=d}^{2d-1} b^i\, \mathscr{A}_i|_g, \sum_{j=d}^{2d-1} c^j\, \mathscr{A}_j\big|_g \right) = \beta^2 b^d c^d + \sum_{i=d+1}^{2d-1} b^i c^i, \end{aligned} \quad (5.14)$$

for all $\mathbf{b} = (b^i)_{i=d}^{2d-1}, \mathbf{c} = (c^i)_{i=d}^{2d-1} \in \mathbb{R}^d$. So by construction the horizontal left-invariant vector fields $\{\mathscr{A}_i\}_{i=d}^{2d-1}$ form an orthonormal basis in Δ_d w.r.t. metric tensor G_1.

5.1.2 *Lifting Problem* $\mathbf{P}_{\mathbf{curve}}$ *to Problem* $\mathbf{P}_{\mathbf{mec}}$ *on* $(SE(d), \Delta_d, G_\beta)$

Now we relate the problem $\mathbf{P}_{\mathbf{curve}}$ to a sub-Riemannian problem $\mathbf{P}_{\mathbf{mec}}$ on the Lie group quotient $\mathbb{R}^d \rtimes S^{d-1}$ given by Eq. (5.6). We define this sub-Riemannian problem by means of the left-invariant frame $\{\mathscr{A}_i\}_{i=d}^{d(d+1)/2}$, recall Eq. (5.11), and its left-invariant co-frame $\{\omega^i\}_{i=1}^{d(d+1)/2}$ given by Eq. (5.12). Within this frame, we will consider the horizontal part only, where we recall that the d-dimensional distribution Δ_d is given by Eq. (5.14) where indices run from d to $2d-1$. See Figure 5.4 for a visualization of this left-invariant frame in case $d = 3$. We will define $\mathbf{P}_{\mathbf{mec}}$ on the sub-Riemannian manifold $(SE(d), \Delta_d, G_\beta)$, with distribution Δ_d and metric tensor G_β given by Eq. (5.14), i.e.

$$G_\beta = \beta^2 \omega^d \otimes \omega^d + \sum_{i=d+1}^{2d-1} \omega^i \otimes \omega^i.$$

In the geometric control problem $\mathbf{P}_{\mathbf{mec}}$ on $SE(d)$, we use the sub-Riemannian arc-length parameter t. In $\mathbf{P}_{\mathbf{mec}}$, we aim for curves $\gamma : [0,T] \to SE(d)$, with prescribed boundary conditions $\gamma(0) = (\mathbf{0}, I)$ and $\gamma(T) = (\mathbf{x}_1, R_{\mathbf{n}_1})$, such that

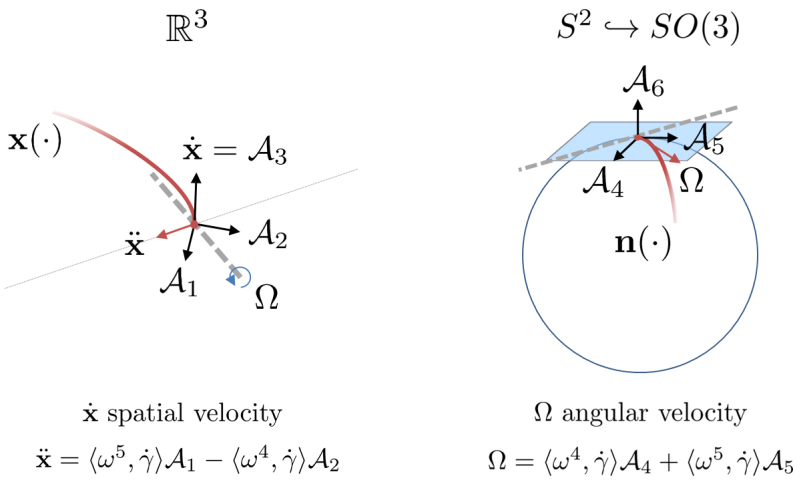

Fig. 5.4 Illustrations of the left invariant frame representing a moving frame of reference along a curve on $\mathbb{R}^3 \rtimes S^2$, i.e. $d = 3$. The spatial velocity and the angular velocity are depicted in the frame to highlight the constraints between the spatial and angular frame.

$$\int_0^T \sqrt{G_\beta|_{\gamma(t)}(\dot{\gamma}(t), \dot{\gamma}(t))}\, \mathrm{d}t = \int_0^T \sqrt{\beta^2 \left(u^d(t)\right)^2 + \sum_{i=d+1}^{2d-1} (u^i(t))^2}\, \mathrm{d}t \qquad (5.15)$$
$$\rightarrow \text{minimize (with free } T)$$

with

$$\dot{\gamma}(t) = \sum_{i=d}^{2d-1} u^i(t) \mathscr{A}_i|_{\gamma(t)} = \sum_{i=d}^{2d-1} \langle \omega^i|_{\gamma(t)}, \dot{\gamma}(t) \rangle \mathscr{A}_i|_{\gamma(t)}$$

where, $u^i \in \mathbb{L}_1([0,T])$ for $i = d, \ldots, 2d-1$ and $R_{\mathbf{n}_1} \in SO(d)$ is any rotation such that $R_{\mathbf{n}_1}\mathbf{a} = \mathbf{n}_1$. In particular, we only consider the stationary curves for which the absolute curvature is $\mathbb{L}_1$ rather than $\mathbb{L}_\infty$.

The existence of minimizers for the problem $\mathbf{P}_{\mathbf{mec}}$ is guaranteed by the theorems by Chow-Rashevskii and Filippov on sub-Riemannian structures [1]. We consider those boundary conditions, for which a minimizer of $\mathbf{P}_{\mathbf{mec}}$ does not admit an internal cusp (i.e. an interior point with infinite curvature). Clearly, such minimizers are also geodesics. We have the following important remarks about these minimizers.

Remark 5.3.
- We have that for $\mathbf{P}_{\mathbf{mec}}$, there are no abnormal extremals. It follows from the fact that any sub-Riemannian manifold with a 2-generating distribution does not allow abnormal extremals (see Chapter 20.5.1 in [1]). This is the case, since for $\Delta_d := \{\mathscr{A}_d, \ldots, \mathscr{A}_{2d-1}\}$ we have $\dim(\Delta_d + [\Delta_d, \Delta_d]) = d(d+1)/2 = dim(SE(d))$.
- Due to the non-existence of abnormal extremals, the minimizers are always analytic [1].

Remark 5.4. Geodesics of $\mathbf{P}_{\mathbf{mec}}$ may lose local and/or global optimality after the end condition at a conjugate point, or global optimality at a Maxwell point. A Maxwell point is a point $\gamma(t)$ on a sub-Riemannian geodesic γ such that $\gamma(t) = \tilde{\gamma}(t)$ for another extremal trajectory $\tilde{\gamma}$ with initial condition satisfying $\tilde{\gamma}(0) = \gamma(0)$. A conjugate point on the other hand is a critical point of the exponential map underlying the geometric control problem (cf. Theorem 21.11 in [1]). Here the exponential map maps each allowable pair $(\lambda(0), \ell)$, with initial momentum $\lambda(0)$ and length ℓ, to the endpoint $\gamma(\ell)$ of the corresponding cuspless sub-Riemannian geodesic $s \mapsto \gamma(s)$ that arises from integrating the canonical Euler-Lagrange or Hamiltonian equations (e.g. obtained via the Pontryagin Maximum Principle). We will provide explicit tangible formulas for this exponential map in case $d \in \{2,3\}$.

Remark 5.5. Throughout this article we will associate to a curve γ in $(SE(d), \Delta_d, G_\beta)$ a corresponding curve $\overline{\gamma}$ in $\mathbb{R}^d \rtimes S^{d-1}$ by setting

$$\begin{aligned} &(SE(d), \Delta_d, G_\beta) \ni \gamma(s) = (\mathbf{x}(s), R(s)) \to \\ &\overline{\gamma}(s) := (\mathbf{x}(s), \mathbf{n}(s)) \in \mathbb{R}^d \rtimes S^{d-1}, \text{ with } \mathbf{n}(s) := R(s)\mathbf{a}. \end{aligned} \tag{5.16}$$

In the remainder of this article, we will write $\gamma(s)$ both for curves in $(SE(d), \Delta_d, G_\beta)$ and for its associated curve in $\mathbb{R}^d \rtimes S^{d-1}$ as it is clear from the context what is meant.

The energy functional in Problem $\mathbf{P}_{\mathbf{curve}}$ and Problem $\mathbf{P}_{\mathbf{mec}}$ coincide for arc-length parameterizable curves $\gamma(\cdot) = (\mathbf{x}(\cdot), R(\cdot))$ in $(SE(d), \Delta_d, G_\beta)$, as we have

$$\begin{aligned} &\sum_{i=d+1}^{2d-1} |\langle\, \omega^i\big|_{\gamma(s)}, \dot{\gamma}(s)\rangle|^2 = \|\underline{\kappa}(s)\|^2 = \kappa^2(s), \\ &\langle\, \omega^d\big|_{\gamma(s)}, \dot{\gamma}(s)\rangle = \|\dot{\mathbf{x}}(s)\| = 1, \end{aligned} \tag{5.17}$$

where $\underline{\kappa}(s) = \ddot{\mathbf{x}}(s)$ denotes the curvature vector and $\kappa(s)$ the curvature magnitude at $\mathbf{x}(s)$ along the spatial part $\mathbf{x}$ of the curve γ.

Remark 5.6. Stationary curves of Problem $\mathbf{P}_{\mathbf{curve}}$ and the spatial part of stationary curves of Problem $\mathbf{P}_{\mathbf{mec}}$ coincide if the end-condition $(\mathbf{x}_1, \mathbf{n}_1) \in \mathbb{R}^d \rtimes S^{d-1}$ is chosen such that it can be connected by a stationary curve of $\mathbf{P}_{\mathbf{curve}}$ (i.e. if the end condition is contained within the range $\mathfrak{R}$ of the exponential map of Problem $\mathbf{P}_{\mathbf{curve}}$).
From now on, such end conditions will be called *admissible end conditions*. E.g. for $d = 2$, we have shown [8] that for each admissible end condition, Problem $\mathbf{P}_{\mathbf{curve}}$ is well-posed and there exists a unique stationary curve connecting the origin $(\mathbf{0}, \mathbf{a})$ with $(\mathbf{x}_1, \mathbf{n}_1)$ that is the global minimum of Problem $\mathbf{P}_{\mathbf{curve}}$. Furthermore, in [15] we have explicitly derived the set of admissible conditions $\mathfrak{R}$. We will summarize these results in Section 5.3.

5.1.3 Structure of the Article

In Section 5.2, we will derive general results for (cuspless) sub-Riemannian geodesics in $(\mathbb{R}^d \rtimes S^{d-1}, \Delta_d, G_\beta)$. We apply the Pontryagin maximum principle and we will show that for cuspless sub-Riemannian geodesics, the phase portrait of momentum reduces to a d-fold planar hyperbolic phase portrait. We express their momentum in terms of the initial momentum accordingly. We show that momentum is parallel transported along the geodesics w.r.t. a Cartan connection, and we derive a theorem allowing explicit integration to the sub-Riemannian geodesics from their momentum. Finally, we show that cuspless sub-Riemannian geodesics are a good model for association fields obtained in neurophysiology and neuropsychology.

In Section 3, we consider the special case $d = 2$, where we derive the unique globally optimal cuspless sub-Riemannian geodesics and their properties. We also carefully analyze the set $\mathfrak{R}$ of admissible end conditions, which is contained in $x \geq 0$, and for which we solve the boundary value problem associated with Problem $\mathbf{P}_{\mathbf{curve}}$ via a semi-analytic method, allowing for a *1D* numerical shooting algorithm to solve the boundary value problem. We also obtain a description and computation of the piecewise smooth boundary $\partial\mathfrak{R}$. From this description we deduce that the extreme orientations per positions are given by endpoints of geodesics ending in a cusp and/or departing from a cusp.

In Section 4, we consider the special case $d = 3$, where we explicitly derive the stationary curves for admissible end conditions (allowing a connection via cuspless sub-Riemannian geodesics). We express their torsion and curvature in terms of momentum, from which we deduce a wide range of geometrical properties. E.g. we show that if the boundary-conditions are co-planar, we obtain the sub-Riemannian geodesics with $d = 2$. Numerical computations show that the sub-Riemannian geodesics are again contained within cones determined by endpoints of those geodesics that end and/or depart from a cusp, supporting (together with the co-planarity results) our *conjecture* that the exponential map of the geometric control problem has similar homeomorphic and diffeomorphic properties as in the case $d = 2$, leaving a challenging open problem for future research. Furthermore, we show that the extreme sub-Riemannian geodesics departing from a cusp will be contained entirely in the half-plane $z \geq 0$.

In Section 5 we consider the special case $d = 4$, where we explicitly derive momentum of the stationary curves.

5.2 Sub-Riemannian Geodesics in $(\mathbb{R}^d \rtimes S^{d-1}, \Delta_d, G_1)$

A general well-established tool to deal with geometric control problems, following a Hamiltonian approach, is the Pontryagin Maximum Principle (PMP) [1, 43, 55]. In Appendix A, we formally apply the Pontryagin maximum principle to problem $\mathbf{P}_{\mathbf{mec}}$ of finding sub-Riemannian geodesics in the sub-Riemannian manifold $(SE(d), \Delta_d, G_1)$. There we also include techniques from theoretical mechanics, following a Lagrangian optimization approach as proposed by [10, 11] which produces

the same canonical equations, to simplify the canonical equations considerably. The resulting equations are surprisingly simple and structured as we will show next. Let

$$\lambda(t) = \sum_{i=1}^{d(d+1)/2} \lambda_i(t)\ \omega^i\big|_{\gamma(t)} = \sum_{i=1}^{2d-1} \lambda_i(t)\ \omega^i\big|_{\gamma(t)}$$

denote the momentum along the sub-Riemannian geodesics (stationary curves $t \mapsto \gamma(t) = (\mathbf{x}(t), R(t))$) expressed in sub-Riemannian arc-length t. Here,

$$\lambda_i = 0 \text{ for all } 2d \leq i \leq d(d+1)/2 = \dim(SE(d)),$$

since momentum does not contain components in the redundant directions $\omega^{2d} = \omega^{2d+1} = \ldots = \omega^{d(d+1)/2} = 0$, recall Eq. (5.10) and Eq. (5.6). To this end we recall that we are interested in connecting points in the Lie group quotient

$$\mathbb{R}^d \rtimes S^{d-1} = SE(d)/(\{0\} \times SO(d-1)),$$

and the $d(d-1)/2$-dimensional Lie-algebra spanned by $\{\mathscr{A}_{2d}, \ldots, \mathscr{A}_{d(d+1)/2}\}$ is precisely the Lie algebra of the $SO(d-1)$ subgroup (i.e. the Lie-algebra of the stabilizer subgroup of our arbitrarily fixed $\mathbf{a} \in S^{d-1}$). Then the canonical equations are given by

$$\boxed{\begin{aligned} \dot{\gamma}(t) &= \sum_{i=d}^{2d-1} \lambda_i(t)\ \mathscr{A}_i|_{\gamma(t)}\,, \\ \dot{\lambda}_i(t) &= -\sum_{j=d}^{2d-1} \sum_{k=1}^{2d-1} c_{i,j}^k \lambda_k(t) \lambda_j(t), \end{aligned}} \tag{5.18}$$

where the first equation relates to the horizontal part of PMP and the second equation to the vertical part of PMP. These equations can be combined in a single equation using a Cartan connection $\overline{\nabla}$ on a cotangent bundle of the sub-Riemannian manifold $(SE(d), \Delta_d, G_\beta)$ that is derived from a Cartan-Maurer form on the underlying principal fiber bundle (akin to [15, App.C] for $d = 2$ and [30, App.A] for $d = 3$). More explicitly, it turns out that (as we shall prove in Theorem 5.2):

$$\boxed{\overline{\nabla}_{\dot{\gamma}} \lambda = 0 \Leftrightarrow \sum_{i=d}^{2d-1} \left(\dot{\lambda}_i + \sum_{k=1}^{2d-1} \sum_{j=d}^{2d-1} c_{i,j}^k \dot{\gamma}^j \lambda_k \right) \omega^i = 0.}$$

with $\dot{\gamma}^k := \langle\, \omega^k\big|_\gamma, \dot{\gamma} \rangle$, which according to the first equality in (5.18) (i.e. the horizontal part of PMP) is equal to λ_k. Computation of (5.18), where we omit the vanishing structure constants, see (5.13), yields

$$\begin{aligned}
\dot{\lambda}_k(t) &= -\lambda_d(t)\lambda_{2d-k}(t)c^d_{k,2d-k} \text{ for } k = 1\ldots,d-1,\\
\dot{\lambda}_d(t) &= -\sum_{k=1}^{d-1} \lambda_k(t)\lambda_{2d-k}(t)c^k_{d,2d-k},\\
\dot{\lambda}_k(t) &= -\lambda_d(t)\lambda_{2d-k}(t)c^{2d-k}_{k,d} \text{ for } k = d+1,\ldots,2d-1,\\
\dot{\lambda}_k(t) &= 0 \text{ for } k = 2d,\ldots,d(d+1)/2.
\end{aligned} \tag{5.19}$$

Now, only for cusp-less sub-Riemannian geodesics γ of problem $\mathbf{P_{mec}}$, we switch to spatial arc-length parameter s, where we note that along such curves we have

$$t'(s) = \sqrt{|\kappa(s)|^2 + 1} \text{ and } s'(t) = \lambda_d(t) \tag{5.20}$$

which follows from $\|\dot{\mathbf{x}}(s)\| = 1$ and Eq. (5.18). On top of that, we use the cyclic property on the structure constants that holds for structure constants of $SE(d)$:

$$c^d_{k,2d-k} = c^k_{2d-k,d}, \text{ for } k = 1\ldots,d-1,$$

and we obtain the following remarkably simple ODE system

$$\begin{aligned}
\ddot{\overline{\lambda}}_k(s) &= \overline{\lambda}_k(s), \text{ for } k \neq d,\\
(\overline{\lambda}_d(s))\dot{\overline{\lambda}}_d(s) &= -\sum_{k=d+1}^{2d-1} (\overline{\lambda}_k(s))\dot{\overline{\lambda}}_k(s),
\end{aligned} \tag{5.21}$$

where $\overline{\lambda}_k(s) := \lambda_k(t(s))$ for $k = 1\ldots,2d-1$. Then we use the fact (akin to [15,30]) that orbits in the augmented space of position and momentum are contained in the co-adjoint orbits[3] of $SE(d)$, i.e.

$$\sum_{k=1}^{d} |\overline{\lambda_k}(s)|^2 = \sum_{k=1}^{d} |\overline{\lambda_k}(0)|^2 =: \mathfrak{c}^2, \tag{5.22}$$

for all $0 \leq s \leq s_{max}$, where s_{max} will be computed later, and the fact that $\overline{\lambda}_d$ is positive (by Eq. (5.20)) to solve for momentum of cuspless sub-Riemannian geodesics:

$$\begin{aligned}
\overline{\lambda}_k(s) &= \overline{\lambda}_k(0)\cosh(s) + \dot{\overline{\lambda}}_k(0)\sinh(s), \text{ for } k \neq d,\\
\overline{\lambda}_d(s) &= \sqrt{\mathfrak{c}^2 - \sum_{k=1}^{d-1} |\overline{\lambda}(s)|^2}.
\end{aligned} \tag{5.23}$$

Remark 5.7. In the remainder of this article, we will just write $\lambda(s)$ instead of $\overline{\lambda}(s)$. When writing $\dot{\lambda}(s)$, we mean $\frac{d}{ds}\lambda(s)$.

Remark 5.8. Besides preservation law (5.22), we deduce the preservation laws

$$\sum_{i=d}^{2d-1} |\lambda_i|^2 = 1 \text{ and } W(\lambda_i,\lambda_j) := \lambda_i\dot{\lambda}_j - \lambda_j\dot{\lambda}_i = \lambda_i(0)\dot{\lambda}_j(0) - \lambda_j(0)\dot{\lambda}_i(0), \tag{5.24}$$

[3] Conservation law (5.22) can also be deduced from the second part of Eq.(5.21).

where W denotes the (constant) Wronskian of λ_i and λ_j for each pair $i,j \in \{1,\dots,d-1\}$ with $i \neq j$.

We represent the momentum co-vector $\lambda(s) = \sum_{i=1}^{2d-1} \lambda_i(s)\ \omega^i\big|_{\gamma(s)}$ by storing its components in a row-vector where we split spatial and angular part

$$\underline{\lambda} = (\underline{\lambda}^{(1)}, \lambda_d; \underline{\lambda}^{(2)}),$$

with $\underline{\lambda}^{(1)} = (\lambda_1,\dots,\lambda_{d-1})$ (where the component index increases), $\underline{\lambda}^{(2)} = (\lambda_{2d-1},\dots,\lambda_{d+1})$ (where the component index decreases). Then Eq.(5.21) becomes

$$\begin{aligned}
&\dot{\underline{\lambda}}^{(1)}(s) = \Lambda \underline{\lambda}^{(2)}(s),\\
&\dot{\lambda}_d(s) = -(\lambda_d(s))^{-1} \sum_{k=1}^{d-1} \lambda_k(s)\lambda_{2d-k}(s) c^k_{d,2d-k},\\
&\dot{\underline{\lambda}}^{(2)}(s) = \Lambda \underline{\lambda}^{(1)}(s),
\end{aligned}$$

where $\Lambda = \operatorname{diag}\left(\{c^d_{k,2d-k}\}_{k=1}^{d-1}\right) \in \mathbb{R}^{(d-1)\times(d-1)}$ is a diagonal matrix whose diagonal elements are determined by the vector $\{c^d_{k,2d-k}\}_{k=1}^{d-1}$ whose elements are within $\{-1,1\}$. Since $\Lambda^2 = I$, it produces the solutions

$$\begin{aligned}
&\underline{\lambda}^{(1)}(s) = \underline{\lambda}^{(1)}(0)\cosh(s) + \Lambda \underline{\lambda}^{(2)}(0)\sinh(s),\\
&\lambda_d(s) = \sqrt{1 - \|\underline{\lambda}^{(2)}(s)\|^2} = \sqrt{\mathfrak{c}^2 - \|\underline{\lambda}^{(1)}(s)\|^2},\\
&\underline{\lambda}^{(2)}(s) = \underline{\lambda}^{(2)}(0)\cosh(s) + \Lambda \underline{\lambda}^{(1)}(0)\sinh(s).
\end{aligned} \tag{5.25}$$

In turn, these formulas allows us to compute the arc-length towards a cusp

$$s_{max}(\lambda(0)) = \log\left(\frac{\sqrt{1+\mathfrak{c}^2 + \sqrt{|1+\mathfrak{c}^2|^2 - \|\underline{\lambda}^{(1)}(0) + \Lambda\underline{\lambda}^{(2)}(0)\|\|\underline{\lambda}^{(1)}(0) - \Lambda\underline{\lambda}^{(2)}(0)\|}}}{\|\underline{\lambda}^{(1)}(0) + \Lambda\underline{\lambda}^{(2)}(0)\|} \right), \tag{5.26}$$

since at a cusp, we have $\lambda_d(t_{cusp}) = 0$ and we have

$$\lim_{s\uparrow s_{max}} \|\underline{\lambda}^{(2)}(s)\| = 1 \Leftrightarrow \lim_{s\uparrow s_{max}} |\lambda_d(s)| = 0 \Leftrightarrow \lim_{s\uparrow s_{max}} \kappa(s) \to \infty,$$

recall Eq. (5.20), with $t_{cusp} = t(s_{max})$.

Let us summarize these results on sub-Riemannian geodesics in $(SE(d), \Delta_d, G_1)$ in the following theorems.

Theorem 5.1. *Along the sub-Riemannian geodesics in $(SE(d), \Delta_d, G_1)$, the following canonical equations hold*

$$\begin{aligned} \dot{\gamma}(t) &= \sum_{i=d}^{2d-1} \lambda_i(t)\, \mathscr{A}_i|_{\gamma(t)}\,, \\ \dot{\lambda}_i(t) &= -\sum_{j=d}^{2d-1} \sum_{k=1}^{2d-1} c^k_{i,j} \lambda_k(t)\, \lambda_j(t), \end{aligned} \tag{5.27}$$

along cuspless sub-Riemannian geodesics (i.e. the sub-Riemannian geodesics that allow parametrization by spatial arc-length s) in $(SE(d), \Delta_d, G_\beta)$. Momentum $\lambda = \sum_{i=1}^{2d-1} \lambda_i \omega^i$ satisfies the simple ODE system Eq. (5.21), whose explicit solution is given by Eq. (5.25). The spatial arc-length towards a cups is given by Eq. (5.26).

Proof. For Eq. (5.27), see Appendix A. The remainder of the proof follows by the earlier derivations in between Eq. (5.19) and Eq. (5.26). □

Corollary 5.1. *The momentum orbit $s \mapsto \lambda(s)$ of a sub-Riemannian geodesic $s \mapsto \gamma(s)$ is determined by a d-fold hyperbolic phase portrait, see Figure 5.5,*

$$\frac{d}{ds}\begin{pmatrix} -c^i_{d,2d-i}\lambda_{2d-i}(s) \\ \lambda_i(s) \end{pmatrix} = \begin{pmatrix} 0 & -1 \\ 1 & 0 \end{pmatrix} \begin{pmatrix} -c^i_{d,2d-i}\lambda_{2d-i}(s) \\ \lambda_i(s) \end{pmatrix} \text{ for } i = 1, \ldots, d,$$

and preservation law $\lambda_d(s) = \sqrt{1 - \sum_{i=d+1}^{2d-1} |\lambda_i(s)|^2}$ for all $s \leq s_{max}(\lambda(0))$.

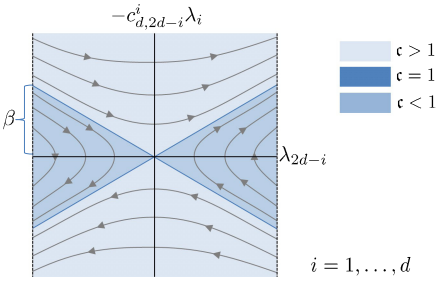

Fig. 5.5 In momentum space, sub-Riemannian geodesics reduce to a d-fold hyperbolic phase portrait, see Corollary 5.1

Theorem 5.2. • *Horizontal exponential curves given by $s \mapsto g_0\, Exp(s \sum_{i=d}^{2d-1} c^i A_i)$, with $c^d = 1$, $g_0 \in SE(d)$, are the auto parallel curves (i.e. $\nabla_{\dot{\gamma}}\dot{\gamma} = 0$) w.r.t. connection $\bar{\nabla}$ on the sub-Riemannian manifold $(SE(d), \Delta_d, G_\beta)$ given by*

$$\bar{\nabla}_X \mathscr{A} = \sum_{k=d}^{2d-1} \left(\dot{a}^k - \sum_{i,j=d}^{2d-1} c_{i,j}^k \dot{\gamma}^i a^j \right) \mathscr{A}_k \tag{5.28}$$

with $X = \sum_{i=d}^{2d-1} \dot{\gamma}^i \mathscr{A}_i$, $\mathscr{A} = \sum_{k=d}^{2d-1} a^k \mathscr{A}_k$.

- *Along an exponential curve, the tangent vectors are covariantly constant, whereas, along a stationary curve, one has covariantly constant momentum, i.e.*

$$\bar{\nabla}_{\dot{\gamma}} \lambda = \sum_{i=1}^{2d-1} \left(\dot{\lambda}_i + \sum_{j=d}^{2d-1} \sum_{k=1}^{2d-1} c_{i,j}^k \lambda_k \dot{\gamma}^j \right) \omega^i = 0.$$

Proof. Define $\dot{\gamma}^i := \langle \omega^i |_\gamma, \dot{\gamma} \rangle$. Then following the same approach as done in [20], [15, App.C] (for the case $d = 2$) and done in [30, App.A] (for the case $d = 3$), the Cartan connection on the tangent bundle is given by Eq. (5.28). From Eq. (5.28), it is directly clear that the auto-parallel curves are horizontal exponential curves, since

$$\begin{aligned} &\bar{\nabla}_{\dot{\gamma}} \dot{\gamma} = 0 \Leftrightarrow \forall_{i \in \{d,\ldots,2d-1\}} \dot{\gamma}^i = 0 \Leftrightarrow \forall_{i \in \{d,\ldots,2d-1\}} \dot{\gamma}^i = c^i \text{ for some constants } c_i \\ &\Leftrightarrow \gamma(s) = \gamma(0) Exp\left(s \sum_{i=d}^{2d-1} c^i A_i \right). \end{aligned}$$

and in order to ensure s to be the spatial arclength parameter we must have $c^d = 1$.

Now the Cartan connection on the tangent bundle naturally imposes the following Cartan connection formula on the co-tangent bundle given by

$$\nabla_{\dot{\gamma}} \sum_{i=1}^{2d-1} \lambda_i \omega^i |_\gamma = \sum_{i=1}^{2d-1} \left(\dot{\lambda}_i + \sum_{j=1}^{2d-1} \sum_{k=1}^{2d-1} c_{i,j}^k \lambda_k \dot{\gamma}^j \right) \omega^i \big|_\gamma \,, \tag{5.29}$$

which follows from Eq. (5.28) and $\mathrm{d}\langle \omega^k |_\gamma, \mathscr{A}_j |_\gamma \rangle = \langle \nabla_{\dot{\gamma}} \omega^k |_\gamma, \mathscr{A}_j |_\gamma \rangle + \langle \omega^k |_\gamma, \nabla_{\dot{\gamma}} \mathscr{A}_j |_\gamma \rangle = 0$. For details see [30, Lemma A.11]. Now, by the horizontal part of PMP (i.e. first equation in Theorem 5.1), we have

$$\dot{\gamma}^j = \lambda_i \text{ for all } i \in \{d, \ldots, 2d-1\},$$

so that the result follows by substituting this equality into Eq. (5.29). □

Now that we have computed momentum $\lambda(s)$ in Theorem 5.1, we can integrate the equation in Theorem 5.2 to find the sub-Riemannian geodesics.

Theorem 5.3. *Let* $m : G \to Aut(\mathbb{R}^{2d})$ *denote the matrix group representation (see Remark 5.9) such that*

$$\mathrm{d}\lambda |_\gamma = \lambda |_\gamma \, m(\gamma^{-1}) \mathrm{d}m(\gamma),$$

where we represent the covector field $\lambda |_\gamma = \sum_{i=1}^{2d-1} \lambda_i \, \omega^i \big|_\gamma$ *along the geodesic* $\gamma(\cdot) = (\mathbf{x}(\cdot), R(\cdot))$, *by a row-vector* $\lambda |_\gamma = (\lambda_1, \ldots, \lambda_{2d}) |_\gamma$, *where we note* $\lambda_{2d} = 0$. *Then along the sub-Riemannian geodesics in* $(SE(d), \Delta_d, G_\beta)$ *the following relation with momentum applies*

$$\lambda(s)m(\gamma(s))^{-1} = \lambda(0)m(\gamma(0))^{-1}.$$

Proof. Note that $\nabla_{\dot\gamma(s)}\, \lambda|_{\gamma(s)} = 0$ iff

$$\frac{d}{ds}\, \lambda(s)|_{\gamma(s)} + \lambda(s)|_{\gamma(s)}\; m((\gamma(s))^{-1})\frac{d}{ds}m(\gamma(s)) = 0$$

for all $0 \leq s \leq s_{max}(\lambda(0))$. The rest follows by

$$\frac{d}{ds}(\lambda(s)(g(s))^{-1}) = -\lambda(s)(g(s))^{-1}\dot\gamma(s)(g(s))^{-1} + \dot\lambda(s)(g(s))^{-1} = 0\,,$$

with $g(s) = m(\gamma(s))$. The last equation must be multiplied with $g(s)$ from the right to obtain the result. □

Remark 5.9. For $d = 2$, this group representation m is given by Eq. (5.33). For $d > 2$ this group representation m is given by

$$m(\mathbf{x}, R) = \begin{pmatrix} R & \sigma_{\mathbf{x}}R \\ 0 & R \end{pmatrix}, \tag{5.30}$$

where $\sigma_{\mathbf{x}} = \sum_{i=1}^{d} x^i A_{d+i} \in \mathrm{so}(d)$, with $\mathbf{x} = \sum_{i=1}^{d} x^i \mathbf{e}_i$ and $A_{d+i} \in \mathrm{so}(d)$. Here, we have $\sigma_{R\mathbf{x}} = R\sigma_{\mathbf{x}}R^{-1}$ and thereby $m(g_1g_2) = m(g_1)m(g_2)$ for all $g_1, g_2 \in SE(d)$. Then

$$\begin{aligned} \mathrm{d}\lambda &= \lambda m(\gamma^{-1})\mathrm{d}m(\gamma) = \lambda \begin{pmatrix} R^{-1}\mathrm{d}R & \sigma_{R^{-1}\mathrm{d}\mathbf{x}} \\ 0 & R^{-1}\mathrm{d}R \end{pmatrix} \\ &= \lambda \begin{pmatrix} \sigma_{(\omega^{d+1},\ldots,\omega^{2d})^T} & \sigma_{(\omega^1,\ldots,\omega^d)^T} \\ 0 & \sigma_{(\omega^{d+1},\ldots,\omega^{2d})^T} \end{pmatrix}, \end{aligned}$$

with short notation $\omega^j = \omega^j\big|_\gamma$, $\lambda = \lambda|_\gamma$, $\mathrm{d}\lambda = \mathrm{d}\lambda|_\gamma$, and where we represent covector $\lambda = \sum_{i=1}^{2d-1} \lambda_i\, \omega^i\big|_\gamma$ by a row-vector $\lambda = (\lambda_1, \ldots, \lambda_{2d})$. Note that $\omega^j\big|_\gamma = 0$ and $\lambda_j = 0$ for all $j \geq 2d$ along sub-Riemannian geodesics $\gamma(\cdot) = (\mathbf{x}(\cdot), R(\cdot))$.

5.2.1 *Summary: The Exponential Map of Control Problem* $\mathbf{P}_{\mathbf{curve}}$

Now let us combine the results of Theorems 5.1, 5.2 and 5.3. Theorem 5.1 provides us momentum $\lambda(s)$ which is entirely determined by $\lambda(0)$. This is not surprising as by Theorem 5.2, one has covariantly constant momentum, as follows from the canonical equations of the Pontryagin maximum principle. The structure of the Cartan connection can be employed to explicitly derive an admissible endpoint $\gamma(\ell)$ of a *cuspless* sub-Riemannian geodesic γ from a pair

$$\begin{aligned} &(\lambda_0, \ell) \in \mathfrak{D} := \{(\lambda_0, \ell) \in \mathscr{C} \times \mathbb{R}^+ \mid \ell \leq s_{max}(\lambda(0)) \neq 0\}, \\ &\text{with } \mathscr{C} := \{\lambda(0) \in T_e^*(SE(d)) \mid \sum_{i=d}^{2d-1} |\lambda_i(0)|^2 = 1\} \end{aligned} \tag{5.31}$$

consisting of momentum λ_0 and length ℓ, with the preservation law of Theorem 5.3. The associated mapping

$$(\lambda_0, \ell) \mapsto \gamma(\ell) =: \widetilde{\mathrm{Exp}}(\lambda_0, \ell)$$

is called exponential map[4] $\widetilde{\mathrm{Exp}}$ of $\mathbf{P}_{\mathbf{curve}}$. It coincides with the exponential map for $\mathbf{P}_{\mathbf{mec}}$ when restricting to admissible end-conditions.

In the subsequent sections we apply this procedure to get an explicit formula for the exponential map $\widetilde{\mathrm{Exp}}$ for the special cases of interest, respectively $d = 2$ and $d = 3$. We will also provide analysis and visualization of the range $\mathfrak{R} := \widetilde{\mathrm{Exp}}(\mathfrak{D})$ of the exponential map and show that it provides a reasonable grouping criterium to connect two points, say $(\mathbf{0}, \mathbf{a})$ and $(\mathbf{x}_1, \mathbf{n}_1)$ within $\mathbb{R}^d \rtimes S^{d-1} := SE(d)/(\{0\} \times SO(d-1))$. This analysis of problem $\mathbf{P}_{\mathbf{curve}}$ (and $\mathbf{P}_{\mathbf{mec}}$ for admissible end-conditions) is related to earlier neuro-psychological models of association fields [26, 41].

5.3 The Case $d = 2$: Sub-Riemannian Geodesics in $(\mathbb{R}^2 \rtimes S^1, \Delta_2, G_1)$

Let us first apply the results regarding sub-Riemannian geodesics within $(\mathbb{R}^d \rtimes S^{d-1}, \Delta_d, G_\beta)$ to the special case $d = 2$. Following our standard conventions, we get

$$\begin{aligned}
&\mathbf{a} := \mathbf{e}_y \text{ and furthermore}\\
&A_1 = \partial_x,\ A_2 = \partial_y,\ A_3 = \partial_\theta,\\
&\mathscr{A}_1 = \cos\theta\,\partial_x + \sin\theta\,\partial_y,\ \mathscr{A}_2 = -\sin\theta\,\partial_x + \cos\theta\,\partial_y,\ \mathscr{A}_3 = \partial_\theta,\\
&\omega^1 = \mathrm{d}\theta, \omega^2 = \cos\theta\,\mathrm{d}x + \sin\theta\,\mathrm{d}y, \omega^3 = -\sin\theta\,\mathrm{d}x + \cos\theta\,\mathrm{d}y,\\
&\Delta_2 = \mathrm{span}\{\mathscr{A}_2, \mathscr{A}_3\},\\
&G_\beta = \omega^3 \otimes \omega^3 + \beta^2 \omega^2 \otimes \omega^2 \text{ where we set } \beta = 1.
\end{aligned}$$

This produces the following canonical ODE-system for momentum $\lambda = \sum_{i=1}^{3} \lambda_i \omega^i$ along the sub-Riemannian geodesics:

$$\dot{\lambda}_1(t) = \lambda_2(t)\lambda_3(t),\ \dot{\lambda}_2(t) = -\lambda_1(t)\lambda_3(t),\ \dot{\lambda}_3(t) = \lambda_1(t)\lambda_2(t),$$

expressed in sub-Riemannian arclength parameter t. Along *cuspless* sub-Riemannian geodesics, this ODE-system simplifies to

$$\dot{\lambda}_1(s) = -\lambda_3(s),\ \dot{\lambda}_2(s) = -\tfrac{\lambda_1(s)\lambda_3(s)}{\lambda_2(s)},\ \dot{\lambda}_3(s) = -\lambda_1(s),$$

using the spatial arc-length parameter s, and we find preservation laws

$$\lambda_1^2 + \lambda_2^2 = \mathfrak{c}^2 := \lambda_1^2(0) + \lambda_2^2(0),\ \lambda_2^2 + \lambda_3^2 = 1,$$

[4] In our notation of the exponential map, we include a tilde to avoid possible confusion with the exponential map $Exp : T_e(G) \to G$ from Lie algebra to Lie group.

and solutions

$$\begin{aligned}
\lambda_1(s) &= \lambda_1(0)\cosh(s) - \lambda_3(0)\sinh(s),\\
\lambda_2(s) &= \sqrt{1-|\lambda_3(s)|},\\
\lambda_3(s) &= \tfrac{d\theta}{dt}(t(s)) = \tfrac{\kappa(s)}{\sqrt{\kappa^2(s)+1}} = \lambda_3(0)\cosh s - \lambda_1(0)\sinh s,
\end{aligned}$$

where $\kappa(s)$ denotes the curvature of the spatially projected curve $s \mapsto (x(s), y(s))$. The maximum length towards a cusp is given by

$$s_{max}(\lambda(0)) = \log \frac{1+\mathfrak{c}}{|\lambda_1(0) - \lambda_3(0)|}, \tag{5.32}$$

with $\mathfrak{c} = \sqrt{|\lambda_1(0)|^2 + |\lambda_2(0)|^2}$. Let $m : SE(2) \to \mathbb{R}^{3\times 3}$ be given by

$$m(x,y,\theta) = \begin{pmatrix} \cos\theta & \sin\theta & -x \\ -\sin\theta & \cos\theta & y \\ 0 & 0 & 1 \end{pmatrix}. \tag{5.33}$$

Then along the geodesics we have

$$\lambda(s)\, m(\gamma(s)) = \lambda(0)\, m(\gamma(0)) = \lambda(0) \text{ for all } s \in [0, s_{max}(\lambda(0))),$$

which allows us to compute the endpoint $\gamma(s) = (x(s), y(s), \theta(s)) \in SE(2)$ of a *cuspless* sub-Riemannian geodesic from a pair $(s, \lambda(0))$ with $s \leq s_{max}(\lambda(0))$.

5.3.1 *Switching to the Case* $\mathbf{a} = \mathbf{e}_x$ *and Re-labeling of the Lie-Algebra*

So far we have applied the general formula for sub-Riemannian geodesics within $(\mathbb{R}^d \rtimes S^{d-1}, \Delta_d, G_1)$ to the special case $d = 2$, where we kept track of consistency with the case $d \geq 3$.

However, in order to directly relate to previous works by the authors on sub-Riemannian geodesics within the 2D-Euclidean motion group and orientation scores [19, 20], we will in the remainder of this section switch to the case $\mathbf{a} = \mathbf{e}_x$ (instead of $\mathbf{a} = \mathbf{e}_y$), and we will re-label the Lie-algebra as follows:

$$\mathscr{A}_1 := \partial_\theta, \quad \mathscr{A}_2 := \cos\theta\partial_x + \sin\theta\partial_y, \quad \mathscr{A}_3 := -\sin\theta\partial_x + \cos\theta\partial_y. \tag{5.34}$$

The corresponding dual vectors are given by

$$\omega^1 := \mathrm{d}\theta, \quad \omega^2 := \cos\theta\mathrm{d}x + \sin\theta\mathrm{d}y, \quad \omega^3 := -\sin\theta\mathrm{d}x + \cos\theta\mathrm{d}y, \tag{5.35}$$

that we will use to represent the momentum covector $\lambda = \sum_{i=1}^{3} \lambda_i \omega^i$ accordingly.

5.3.2 Explicit Parameterizations of the Cuspless Sub-Riemannian Geodesics and Their Properties

Let us explicitly compute the exponential map for the case $d = 2$ using spatial arc-length parametrization which provides us an explicit formula for the sub-Riemannian geodesics in $(SE(2), \Delta_2, G_1)$ (recall Remark 5.2). We will use the labeling/ordering conventions (5.34) and (5.35).

Theorem 5.1 directly provides us the linear ODE

$$\ddot{\lambda}_1(s) = \lambda_1(s) \Leftrightarrow \frac{d^2}{ds^2}\left(\frac{\kappa(s)}{\sqrt{\kappa^2(s)+1}}\right) = \frac{\kappa(s)}{\sqrt{\kappa^2(s)+1}},$$

which directly provides us with the curvature $\kappa(s)$ of the cuspless sub-Riemannian geodesics in terms of $\lambda(0) = \lambda_1(0)\mathrm{d}\theta + \lambda_2(0)\mathrm{d}x + \lambda_3(0)\mathrm{d}y$ and spatial arc-length s, with $s \leq s_{max}(\lambda(0))$, recall Eq. (5.32). Now instead of integrating a Frenet ODE system, we apply an effective integration procedure via Theorem 5.3. We have

$$\mathrm{d}\hat{\lambda} = \hat{\lambda}\,(m(\gamma))^{-1}\mathrm{d}m(\gamma) \Leftrightarrow \hat{\lambda}(s)\,m(\gamma(s)) = \hat{\lambda}(0)\,m(\gamma(0)) = \hat{\lambda}(0), \tag{5.36}$$

where we use short notation for the row-vector

$$\hat{\lambda} := (-\lambda_3(s), \lambda_2(s), \lambda_1(s)) = (\dot{\lambda}_1(s), \frac{1}{\sqrt{\kappa^2(s)+1}}, \frac{\kappa(s)}{\sqrt{\kappa^2(s)+1}}) \tag{5.37}$$

with $m(\gamma) = \begin{pmatrix} \cos\theta & -\sin\theta & x \\ \sin\theta & \cos\theta & y \\ 0 & 0 & 1 \end{pmatrix}$ the most common group representation of $SE(2)$.

Lemma 5.1. *Let* $\mathfrak{c} := \sqrt{|\lambda_2(0)|^2 + |\lambda_3(0)|^2}$. *There exists a unique* $h_0 \in SE(2)$ *such that* $\hat{\lambda}(0)m(h_0^{-1}) = (\mathfrak{c}, 0, 0)$. *Consequently, we have for* $\tilde{\gamma}(s) := h_0\gamma(s)$ *that*

$$(-\lambda_3(s), \lambda_2(s), \lambda_1(s)) = \hat{\lambda}(s) = (\mathfrak{c}\ 0\ 0)\ m(\tilde{\gamma}(s)). \tag{5.38}$$

Proof. Follows by Theorem 5.3 and the fact that m is a group representation. □

Application of this lemma provides the following explicit formula for the sub-Riemannian geodesics in $(SE(2), \Delta_2, G_1)$.

Theorem 5.4. *The exponential map of* $\mathbf{P}_{\mathbf{curve}}$ *expressed in spatial arc-length parametrization is given by*

$$\begin{aligned} &\widetilde{Exp}\left(\sum_{i=1}^{3} \lambda_i(0)\ \omega^i\big|_{\gamma(0)=e}\ ,\ s\right), \\ &= \gamma(s) = (x(s), y(s), \theta(s)), \end{aligned} \tag{5.39}$$

for all $s \in [0, \ell]$ *with total spatial length* $\ell \leq s_{max}(\lambda(0))$. *The cuspless geodesics in* $(SE(2), \Delta_2, G_1)$ *are given by* $\gamma(s) = h_0^{-1}\tilde{\gamma}(s)$, *i.e.*

$$\begin{aligned}
&\theta(s) = \tilde{\theta}(s) - \overline{\theta}_0 \in [-\pi, \pi],\\
&\text{with } \cos(\overline{\theta}_0) = \tfrac{-\lambda_3(0)}{\mathfrak{c}} \text{ and } \overline{\theta}_0 \in [-\pi, 0],\\
&\mathbf{x}(s) = \overline{R}_0^T \left(\tilde{\mathbf{x}}(s) - \overline{\mathbf{x}}_0\right),\\
&\text{with } \overline{R}_0^T = \begin{pmatrix} \cos\overline{\theta}_0 & \sin\overline{\theta}_0 \\ -\sin\overline{\theta}_0 & \cos\overline{\theta}_0 \end{pmatrix} = \tfrac{1}{\mathfrak{c}} \begin{pmatrix} -\lambda_3(0) & -\lambda_2(0) \\ \lambda_2(0) & -\lambda_3(0) \end{pmatrix}
\end{aligned} \tag{5.40}$$

with $h_0 = (\overline{\mathbf{x}}_0, \overline{R}_0) \in SE(2)$, $\overline{\mathbf{x}}_0 = (\frac{-\lambda_3(0)}{\mathfrak{c}}, 0)^T$. *Here curve* $\tilde{\gamma} = (\tilde{x}, \tilde{y}, \tilde{\theta})$ *is given by*

$$\begin{aligned}
&\tilde{x}(s) = \tfrac{\lambda_1(s)}{\mathfrak{c}} = \tfrac{\lambda_1(0)\cosh(s) - \lambda_3(0)\sinh(s)}{\mathfrak{c}},\\
&\tilde{y}(s) = -\tfrac{1}{\mathfrak{c}} \int_0^s \sqrt{1 - |\lambda_1(\tau)|^2}\, \mathrm{d}\tau,\\
&\tilde{\theta}(s) = \arg(\dot{\tilde{x}}(s) + i\dot{\tilde{y}}(s))\\
&\quad = \arg(-\lambda_3(s) - i\lambda_2(s)) \in [-\pi, 0],
\end{aligned} \tag{5.41}$$

with $\lambda_1(s) = \lambda_1(0)\cosh s - \lambda_3(0)\sinh s$, $\lambda_3(s) = \lambda_3(0)\cosh s - \lambda_1(0)\sinh s$ *and where* $\mathfrak{c} = \sqrt{|\lambda_2(0)|^2 + |\lambda_3(0)|^2} \geq 0$.

From these formulas one can directly deduce the following properties:

- If $\mathfrak{c} \leq 1$, the curvature does not switch sign and we obtain U-shaped curves, unless $\lambda_1(0) = \lambda_3(0) = 0$ in which case we get a straight line.
- If $\mathfrak{c} > 1$ and $\lambda_1(0)\lambda_3(0) > 0$, then the curve is an S-shaped curve with bending-point at $s_B = \log \frac{\|\lambda_1(0) + \lambda_3(0)\|}{\|\lambda_1(0) - \lambda_3(0)\|}$.
- If $\mathfrak{c} = 1$ and $\lambda_3(0) = \lambda_1(0)$ we have $s_{max} = \infty$.
- The cuspless sub-Riemannian geodesics are monotonically increasing along the $\lambda_2(0)\mathbf{e}_x + \lambda_3(0)\mathbf{e}_y$-axis:

  $$-\dot{\tilde{y}}(s) \geq 0 \Leftrightarrow \lambda_2(0)\dot{x}(s) + \lambda_3(0)\dot{y}(s) \geq 0,$$

  and even if they tend towards a cusp where curvature tends to infinity, they do not roll up and their sub-Riemannian length stays finite.
- The cuspless sub-Riemannian geodesics are contained within the half-space $x \geq 0$ and the boundary $x = 0$ can only be reached with an angle (w.r.t. the positive x-axis) of π as formally proven in [15, Thm.7 and Thm.8].

5.3.3 The Set $\mathfrak{R}$ and Its Boundary $\partial\mathfrak{R}$

Now that we have computed the exponential map, let us have a look at the range $\mathfrak{R} = \widetilde{\mathrm{Exp}}(\mathfrak{D})$, which according to the results in [8] coincides precisely with the points for which $\mathbf{P}_{\mathbf{curve}}$ admits a global minimum. In fact, we have

Theorem 5.5. *In* $\mathbf{P}_{\mathbf{curve}}$ *with* $d = 2$, *we set initial condition* $(x_{in}, y_{in}, \theta_{in}) = e = (0,0,0)$ *and consider* $(x_{fin}, y_{fin}, \theta_{fin}) \in \mathbb{R}^2 \rtimes S^1$. *Then*

- $(x_{fin}, y_{fin}, \theta_{fin}) \in \mathfrak{R}$ *if and only if* $\mathbf{P}_{\mathbf{curve}}$ *has a unique minimizing geodesic which exactly coincides with the unique minimizer of* $\mathbf{P}_{\mathbf{mec}}$.

- $(x_{fin}, y_{fin}, \theta_{fin}) \notin \mathfrak{R}$ *if and only if problem* $\mathbf{P_{curve}}$ *is ill-defined (i.e.* $\mathbf{P_{curve}}$ *does not have a minimizer).*

Corollary 5.2. *Set* $g_{in} = e$. *Then* g_{fin} *is an admissible end-condition for* $\mathbf{P_{curve}}$ *if* $g_{fin} \in \mathfrak{R}$.

According to the next theorem the exponential map has nice smoothness and bijection properties and properly maps analytic trajectories in the hyperbolic phase portrait in momentum space onto analytic sub-Riemannian geodesics in $(SE(2), \Delta_2, G_1)$. For a visualization on how this is achieved physically, see Figure 5.6.

Theorem 5.6. *Let* $\mathfrak{D}$ *and* $\mathfrak{R}$ *denote respectively the domain and range of the exponential map of* $\mathbf{P_{curve}}$ *defined on* $(SE(2), \Delta_2, G_1)$. *Then,*

- $\widetilde{Exp} : \mathfrak{D} \to \mathfrak{R}$ *is a homeomorphism if we equip* $\mathfrak{D}$ *and* $\mathfrak{R}$ *with the subspace topology*[5].
- $\widetilde{Exp} : \mathring{\mathfrak{D}} \to \mathring{\mathfrak{R}}$ *is a diffeomorphism.*

Finally, the boundary $\partial\mathfrak{R}$ *is given by*

$$\partial\mathfrak{R} = \mathscr{S}_B \cup \mathfrak{l} \cup \mathscr{S}_R, \tag{5.42}$$

with $\mathfrak{l} := \{(0,0,\theta) \mid -\pi \leq \theta \leq \pi\}$ *the sphere above the spatial origin,*

$$\mathscr{S}_B := \{\widetilde{Exp}(\lambda_0, s_{max}(\lambda_0)) \mid \lambda_0 \in \mathscr{C}\} \tag{5.43}$$

the set of endpoints of geodesics ending at a cusp (the blue surfaces in Fig. 5.6), and

$$\mathscr{S}_R := \left\{\widetilde{Exp}(\lambda_0, s) \,|\, \lambda_0 \in \mathscr{C} \text{ with } \lambda_3(0) = \pm 1 \text{ and } s \in (0, s_{max}(\lambda(0))\right\} \tag{5.44}$$

the set of endpoints of geodesics departing from a cusp (the red surfaces in Fig. 5.6).

Proof. See [15, App.F].

As a result the set $\mathfrak{R}$ is a connected set with a piecewise smooth boundary $\partial\mathfrak{R}$ given by Eq. (5.42). In fact, when taking the intersection with $\{(\mathbf{x}_1, \mathbf{n}) \mid \mathbf{n} \in S^1\}$ with $\mathbf{x}_1 = (x_{fin}, y_{fin}) \in \mathbb{R}^2$ fixed we get a cone in S^1. Sometimes this cone is bounded by a red and a blue surface and sometimes it is bounded by the blue surfaces in Figure 5.6. Also see Figure 5.7.

Let us underpin this observation on the cone of reachable angles with a formal theorem. To this end let $\theta_{\text{endcusp}}(x_{fin}, y_{fin})$ denote the final angle (w.r.t. the positive x-axis) of the geodesic ending in $(x_{fin}, y_{fin}, \cdot)$ with a cusp and where

[5] As $\mathfrak{D}$ and $\mathfrak{R}$ are not open w.r.t. standard topologies on the embedding spaces $T_e(SE(2)) \times \mathbb{R}^+$ and $\mathbb{R}^2 \times S^1$, these subspace topologies do not coincide with the induced topology imposed by the embedding via the identity map. W.r.t. the subspace topologies the set $\mathfrak{D}$, respectively $\mathfrak{R}$, are open sets and the homeomorphism $\widetilde{\text{Exp}} : \mathfrak{D} \to \mathfrak{R}$ is well-defined.

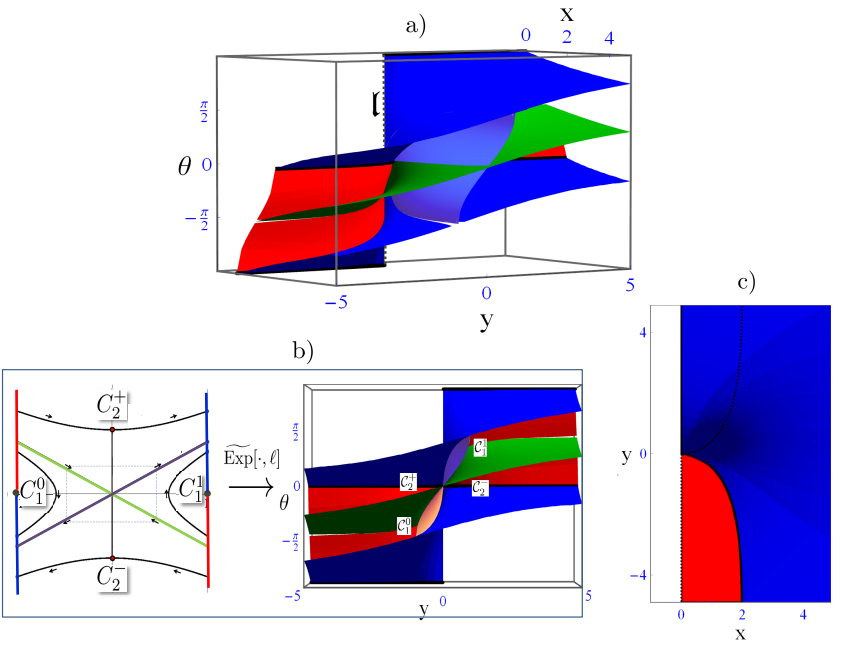

Fig. 5.6 Plots (from 3 perspectives a), b) and c)) of the range $\mathfrak{R}$ of the exponential map of $\mathbf{P}_{\mathbf{curve}}$. Red surface: endpoints of geodesics starting from cusps. Blue surface: endpoints of geodesics ending in cusps. The black lines are the intersections of the blue plane with the red plane. Green surface: critical surface ($\mathfrak{c} = 1$) with $\dot{z}_0 = -z_0$. Purple surface: critical surface ($\mathfrak{c} = 1$) with $\dot{z}_0 = z_0$. The critical surface splits the range of the exponential map into four disjoint parts $\mathscr{C}_1^1$, $\mathscr{C}_1^0$, $\mathscr{C}_2^+$ and $\mathscr{C}_2^-$ that relate to the splitting of the phase space into C_1^1, C_1^0, C_2^+ and C_2^- in b) where we have depicted $\mathfrak{R}$ viewed from the x-axis. In c) we have depicted $\mathfrak{R}$ viewed from the θ-axis.

$\theta_{\text{begincusp}}(x_{fin}, y_{fin})$ denotes the final angle of a geodesic ending in $(x_{fin}, y_{fin}, \cdot)$ starting with a cusp. In case there exist two geodesics ending with a cusp at (x_{fin}, y_{fin}), we order them by writing

$$\theta^1_{\text{endcusp}}(x_{fin}, y_{fin}) \leq \theta^2_{\text{endcusp}}(x_{fin}, y_{fin}).$$

Theorem 5.7. *Let* $(x_{fin}, y_{fin}, \theta_{fin}) \in \mathfrak{R}$. *If*

$$|y_{fin}| \leq -x_{fin}\, iE\left(i \operatorname{arcsinh} \frac{x_{fin}}{\sqrt{4 - x_{fin}^2}}, \frac{x_{fin}^2 - 4}{x_{fin}^2}\right), \quad \textit{and} \quad 0 \leq x_{fin} < 2. \tag{5.45}$$

then we have

$$y_{fin} > 0 \Rightarrow \theta_{fin} \in [\theta_{begincusp}(x_{fin}, y_{fin}), \theta_{endcusp}(x_{fin}, y_{fin})],$$

$$y_{fin} < 0 \Rightarrow \theta_{fin} \in [\theta_{endcusp}(x_{fin}, y_{fin}), \theta_{begincusp}(x_{fin}, y_{fin})],$$

otherwise (so in particular if $x_{fin} \geq 2$) we have

$$\theta_{fin} \in [\theta^1_{endcusp}(x_{fin}, y_{fin}), \theta^2_{endcusp}(x_{fin}, y_{fin})].$$

Proof. See [15, App.E]. For a direct graphical validation of Theorem 5.7 see Figure 5.6 (in particular the top view along the θ direction).

5.3.4 Solving the Boundary Value Problem

The inverse of the exponential map $(\lambda_0, \ell) \mapsto \widetilde{\mathrm{Exp}}(\lambda(0), \ell) = \gamma(\ell) = g_{fin}$ in Theorem (5.4) can be computed analytically to a large extent. That is, ℓ, $\lambda_2(0)$, $\lambda_3(0)$ can all be analytically expressed in terms of $-1 \leq \lambda_1(0) \leq 1$, which leaves an accurate and efficient *one dimensional* numerical shooting algorithm to find the final remaining unknown $\lambda_1(0)$, as given by the following theorem. Note that recently proposed numerical approaches in the literature [6, 35] rely on three dimensional numerical shooting algorithms.

Theorem 5.8. *Let $g_{fin} \in \mathfrak{R}$. The inverse of the exponential map $(\lambda_0, \ell) \mapsto \widetilde{Exp}(\lambda(0), \ell) = \gamma(\ell) = g_{fin}$ in Theorem 5.4 is given by*

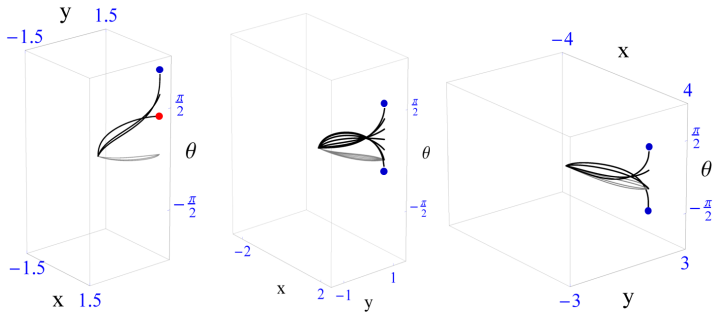

Fig. 5.7 Sub-Riemannian geodesics (and their spatial projections in grey) obtained by our analytical approach to the boundary value problem. We have kept (x_{fin}, y_{fin}) fixed and we have varied θ_{fin} to full range such that our algorithm finds solutions (with relative errors less than 10^{-8}). Left: $(x_{fin}, y_{fin}) = (1, 1.5)$, middle: $(x_{fin}, y_{fin}) = (2, 1)$, right: $(x_{fin}, y_{fin}) = (4, 1)$. At the boundary of cones of reachable angles, the endpoints of the sub-Riemannian geodesics are located on the cusp-surface $\partial\mathfrak{R}$. End-points of geodesics departing from cusps are indicated in red and endpoints of geodesics ending at cusps are indicated in red (as in Figure 5.6).

$$\lambda(0) = \sum_{i=1}^{2} \lambda_i(0)\omega^i,$$
$$\ell(\lambda(0), g_{fin}) = \begin{cases} \log \frac{\lambda_1(0)}{v}, & \mathfrak{c} = 1 \text{ and } \lambda_3(0) = \lambda_1(0), \\ \log \frac{v}{\lambda_1(0)}, & \mathfrak{c} = 1 \text{ and } \lambda_3(0) = -\lambda_1(0), \\ \log \frac{v+w}{\lambda_1(0)-\lambda_3(0)}, & \text{else} \end{cases} \tag{5.46}$$
where $v, w, \mathfrak{c}$ *are given by*
$v = \lambda_1(\ell) = \lambda_1(0) - x_{fin}\lambda_3(0) + y_{fin}\lambda_2(0),$
$w = -\lambda_3(\ell) = -\lambda_3(0)\cos\theta_{fin} + \lambda_2(0)\sin\theta_{fin},$
$\mathfrak{c} = \sqrt{|\lambda_2(0)|^2 + |\lambda_3(0)|^2}.$

Here $\lambda_2(0), \lambda_3(0)$ *are expressed as follows:*

$$\lambda_2(0) = \chi_2(\lambda_1(0)) := \sqrt{1 - |\lambda_1(0)|^2},$$
$$-\lambda_3(0) = \chi_3(\lambda_1(0), g_{fin}) := \frac{-b + sign(g_{fin})\sqrt{D}}{2a},$$
with $a = x_{fin}^2 + \sin^2(\theta_{fin}),$
$b = 2x_{fin}(\lambda_1(0) + y_{fin}\lambda_2(0)) - \lambda_2(0)\sin(2\theta_{fin}),$
$c = |\lambda_2(0)|^2(y_{fin}^2 - \sin^2(\theta_{fin})) + 2y_{fin}\lambda_1(0)\lambda_2(0),$
$D = b^2 - 4ac =: \mathscr{D}(\lambda_1(0), g_{fin}),$

and with sign function given by

$$\text{sign}(g_{\text{fin}}) = \begin{cases} 1 & \text{if } g_{fin} \in \mathscr{C}_2^+, \\ 1 & \text{if } g_{fin} \in \mathscr{C}_1^1 \cup \mathscr{C}_1^0 \text{ is above } \mathscr{V}, \\ -1 & \text{if } g_{fin} \in \mathscr{C}_1^1 \cup \mathscr{C}_1^0 \text{ is below } \mathscr{V}, \\ -1 & \text{if } g_{fin} \in \mathscr{C}_2^-, \end{cases} \tag{5.47}$$

with surface $\mathscr{V} \in SE(2)$ *(corresponding to the solutions with* $\lambda_3(0) = 0$*)*

$$\mathscr{V} = \left\{ \widetilde{Exp}(z_0\omega^1 + \chi_2(z_0)\omega^2, \ell) \mid z_0 \in [-1,1] \text{ and } 0 \le \ell \le s_{max}(z_0\omega^1 + \chi_2(z_0)\omega^2) \right\}.$$

Finally, $\lambda_1(0)$ *denotes the unique root* $F(\lambda_1(0)) = 0$ *of* $F : I \to \mathbb{R}^+$ *defined on*

$$I = \{z_0 \in [-1,1] \mid \mathscr{D}(z_0, g_{fin}) \ge 0\}$$

given by $F(z_0) = \|\widetilde{Exp}(z_0\omega^1 + \chi_2(z_0)\omega^2 + \chi_3(z_0, g_{fin})\omega^3, \ell(z_0, g_{fin})\ ) - g_{fin}\|$, *where* $\|\cdot\|$ *denotes the Euclidean norm on* $\mathbb{R}^2 \times S^1$.

Proof. By Theorem 5.5, there is a unique stationary curve connecting e and $g_{fin} \in \mathfrak{R}$. The exponential map of $\mathbf{P_{curve}}$ is a homeomorphism by Theorem 5.6 and thereby the continuous function F has a unique zero, since ℓ and $\lambda_3(0)$ are already determined by $\lambda_1(0)$ and g_{fin}. W.r.t the formula for ℓ, Theorem 5.1 (for $d=2$) implies that:

$$\lambda_1(\ell) = \lambda_1(0)\cosh\ell - \lambda_3(0)\sinh\ell,\ \lambda_3(\ell) = \lambda_3(0)\cosh\ell - \lambda_1(0)\sinh\ell$$

from which e^ℓ can readily be obtained, noting that (by Theorem 5.4 for $s = \ell$):

$$\lambda_1(\ell) = \lambda_1(0) - x_{fin}\lambda_3(0) + y_{fin}\lambda_2(0),\ -\lambda_3(\ell) = -\lambda_3(0)\cos\theta_{fin} + \lambda_2(0)\sin\theta_{fin}.$$

Finally, applying the preservation laws (recall Remark 5.8) $|\lambda_1(s)|^2 + |\lambda_2(s)|^2 = 1$ and $|\lambda_2(s)|^2 + |\lambda_3(s)|^2 = |\lambda_2(0)|^2 + |\lambda_3(0)|^2$ to the case $s = \ell$ provides a quadratic equation for $\lambda_3(0)$ from which the result follows. For details on the choice of the sign in the solution of this quadratic equation and surface $\mathscr{V}$, we refer to [15, Lem.8]. □

Remark 5.10. Theorem 5.8 allows for fast and accurate computations of sub-Riemannian geodesics, see Figure 5.7 where the computed geodesics are instantly computed with an accuracy of relative $\mathbb{L}_2$-errors in the order of 10^{-8}. For an example of the application of Theorem 5.8 see Figure 5.8. Finally, we note that Theorem 5.6 implies that (our approach to) solving the boundary-value problem is well-posed, i.e. the solutions are both unique and stable.

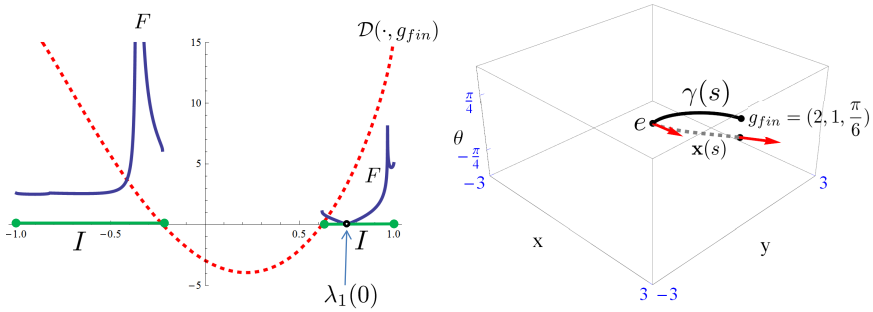

Fig. 5.8 The particular case where $g_{fin} = (2, 1, \pi/6)$, where $\text{sign}(g_{fin}) = -1$ and where unique root of $F(\cdot, g_{fin})$, whose domain I is indicated in green, is approximatively $\lambda_1(0) \approx 0.749551$ (and thereby $\lambda_2(0) = \sqrt{1 - |\lambda_1(0)|^2}$, $\lambda_3(0) \approx -0.809740$ and $L \approx 2.26253$).

5.3.5 *Modeling Association Fields with Solutions of P_{curve}*

Sub-Riemannian geometry plays a major role in the functional architecture of the primary visual cortex (V1) and more precisely its pinwheel structure, cf. [42]. In his paper [42], Petitot shows that the horizontal cortico-cortical connections of V1 implement the contact structure of a continuous fibration $\pi : R \times P \to P$ with base space the space of the retina and P the projective line of orientations in the plane. He applies his model to the Field's, Hayes' and Hess' physical concept of an association field, to several models of visual hallucinations [25] and to a variational model of curved modal illusory contours [33, 38, 54].

In their paper, Field, Hayes and Hess [26] present physiological speculations concerning the implementation of the association field via horizontal connections. They have been confirmed by Jean Lorenceau et al. [34] via the method of apparent speed

of fast sequences, where the apparent velocity is overestimated when the successive elements are aligned in the direction of the motion path and underestimated when the motion is orthogonal to the orientation of the elements. They have also been confirmed by electrophysiological methods measuring the velocity of propagation of horizontal activation [29]. There exist several other low-level vision models and neuro-physiological measurements that have produced similar fields of association and perceptual grouping [31, 39, 58]. For an overview see [42, ch:5.5,5.6].

Subsequently, we discuss three models of the association fields: Legendrian geodesics, cuspless sub-Riemannian geodesics and horizontal exponential curves. W.r.t. the latter model, we recall that horizontal exponential curves [20, 48] in the sub-Riemannian manifold $(SE(2), \Delta_2, G_\beta)$, Eq. (5.14), are given by circular spirals

$$\begin{aligned} &r \mapsto g_0 e^{r(c^1 A_1 + c^2 A_2)} = \\ &\left(x_0 + \tfrac{c^2}{c^1}(\sin(c^1 r + \theta_0) - \sin(\theta_0)), y_0 - \tfrac{c^2}{c^1}(\cos(c^1 r + \theta_0) - \cos(\theta_0)), \theta_0 + r c^1\right), \end{aligned} \tag{5.48}$$

for $c^1 \neq 0$, $g_0 = (x_0, y_0, \theta_0) \in SE(2)$ and all $r \geq 0$. If $c^1 = 0$ they are straight lines:

$$g_0 e^{r c^2 A_2} = (x_0 + r c^2 \cos\theta_0, y_0 + r c^2 \sin\theta_0, \theta_0).$$

Clearly, these horizontal exponential curves reflect the co-circularity model [36].

To model the association fields from neuropsychology and neurophysiology Petitot [42] computes "Legendrian geodesics", [42, ch.6.6.4,eq.49] minimizing Lagrangian $\sqrt{1 + |y'(x)|^2 + |\theta'(x)|^2}$ under the constraint $\theta(x) = y'(x)$. This is directly related[6] to the sub-Riemannian geodesics in

$$((SE(2))_0, \mathrm{Ker}(-\theta\,\mathrm{d}x + \mathrm{d}y), \mathrm{d}\theta \otimes \mathrm{d}\theta + \mathrm{d}x \otimes \mathrm{d}x), \tag{5.49}$$

where $(SE(2))_0$ is the well-known nilpotent Heisenberg approximation ([19, ch:5.4]) of $SE(2)$, which minimize Lagrangian $\sqrt{1 + |\theta'(x)|^2}$ under constraint $\theta(x) = y'(x)$. The drawback of such curves is that they are coordinate dependent and not covariant[7] with rotations and translations. Similar problems arise with B-splines which minimize Lagrangian $1 + |\theta'(x)|^2$ under constraint $\theta(x) = y'(x)$ which are commonly used in vector graphics.

To this end, Petitot [42] also proposed the "circle bundle model" which has the advantage that it is coordinate independent. Its energy integral

$$\int_0^{x_{fin}} \sqrt{1 + |y'(x)|^2 + \frac{|y''(x)|^2}{(1 + |y'(x)|^2)^2}}\,\mathrm{d}x \tag{5.50}$$

[6] The dual basis in $(SE(2))_0$ is equal to $(\mathrm{d}\theta, \mathrm{d}x, -\theta\,\mathrm{d}x + \mathrm{d}y)$ and thereby the sub-Riemannian metric on $(SE(2))_0$ does not include the $|y'(x)|^2$ term.

[7] The corresponding minimization problem (and induced sub-Riemannian distance) is left invariant in $(SE(2))_0$ and not left-invariant in $SE(2)$.

can be expressed as $\int_0^\ell \sqrt{1+\kappa^2}\mathrm{d}s$, where $s \in [0,\ell]$ denotes spatial arc-length parametrization. So in case one restricts problem $\mathbf{P_{curve}}$ to those admissible endpoints that allow a cuspless sub-Riemannian geodesic which can be well-parameterized by $(x,y(x),\theta(x))$ with $\theta(x) = \arctan y'(x)$, this restricted problem coincides with Petitot's circle bundle model of finding sufficiently smooth curves $x \mapsto (x,y(x))$ such that the functional in Eq. (5.50) is minimal.

In Figure 5.9, we have modeled the association field with sub-Riemannian geodesics ($\beta = 1$) and horizontal exponential curves (Eq. (5.48) as proposed in [5,48]). Horizontal exponential curves are circular spirals and thereby rely on "co-circularity", a well-known principle to include orientation context in image analysis, cf. [28,36].

On the one hand, a serious drawback arising in the co-circularity model for association fields is that only the spatial part (x_{fin},y_{fin}) of the end-condition can be prescribed (the angular part is imposed by co-circularity), whereas with geodesics one can prescribe $(x_{fin},y_{fin},\theta_{fin})$ (as long as the ending condition is contained within $\mathfrak{R}$). This drawback is clearly visible in Figure 5.9, where the association field (see a) in Figure 5.9) typically ends in points with almost vertical tangent vectors.

On the other hand, the sub-Riemannian geodesic model describes less accurately the association field by Field and co-workers in the (much weaker) connections to the side (where the co-circularity model is reasonable). One could improve the modeling by varying β, but even then it is hard to approximate large circles: the ODE $\ddot{z} = \beta^2 z$ does not allow z to be constant and one can approximate large circles by resigning to large β.

In the more aligned connections in the association field the sub-Riemannian geodesics model the field lines remarkably well (in comparison to the exponential curves), as can be observed in part b) of Figure 5.9. Moreover, the field curves of the association field end with vertical tangent vectors, and these endpoints are very close to cusp points in the sub-Riemannian geodesics modeling these field lines. Following the general idea of Petitot's work [42] (e.g. the circle bundle model) and the results in this article on the existence set $\mathfrak{R}$, this puts the following conjecture:

Conjecture 5.1. The criterium in our visual system to connect two local orientations, say $g_0 = (x_0,y_0,\theta_0) = (0,0,0)$ and $g_{fin} = (x_{fin},y_{fin},\theta_{fin}) \in SE(2)$, could be modeled by checking whether g_{fin} is within the range $\mathfrak{R}$ of the exponential map.

This conjecture needs further investigation by neuro-physiological experiments. In any case, within the model $\mathbf{P_{curve}}$ (coinciding with Petitot's circle bundle model [42] and the sub-Riemannian model by Citti and Sarti [13,49]) a curve is globally optimal if and only if it is stationary, by the results in [8] (summarized in Theorem 5). Furthermore, the sub-Riemannian geodesics strongly deviate from horizontal exponential curves even if the end condition is chosen such that the co-circularity condition is satisfied (see c) in Figure 5.9).

Remark 5.11. Regarding association field models, we discussed 3 different models:

1. The cuspless sub-Riemannian geodesic model $\mathbf{P_{curve}}$, cf. [6,8,13,20,32], (extending Petitot's circle bundle model [42, ch:6.6.5])

2. The Legendrian geodesic model [42],
3. The horizontal exponential curve model in [48] given by Eq. (5.48).

These models relate as follows:

- The Legendrian geodesics follow from the cuspless sub-Riemannian geodesic model by contracting (e.g. [19]) the sub-Riemannian manifold on $(SE(2), \Delta_2, \mathscr{G}_\beta)$ towards its nilpotent approximation, cf. Eq. (5.49).
- The horizontal exponential curves keep the control variable in $\mathbf{P}_{\mathbf{curve}}$ constant and they are rough local approximations of sub-Riemannian geodesics, see item c) in Figure 7. We also recall Theorem 5.2: The discrepancy between horizontal exponential curves and sub-Riemannian geodesics in $(SE(2), \Delta_2, G_\beta)$ is also intriguing from the differential geometrical viewpoint. Due to the presence of torsion in the Cartan connection auto-parallel curves (i.e. *the straight* curves in $(SE(2), \Delta_2, G_\beta)$ satisfying $\nabla_{\dot\gamma}\dot\gamma = 0$) do not coincide with the sub-Riemannian geodesics (i.e. *the shortest curves* in $(SE(2), \Delta_2, G_\beta)$ satisfying $\nabla_{\dot\gamma}\lambda = 0$).

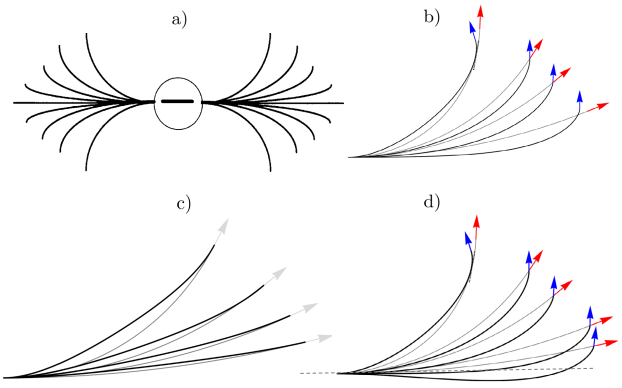

Fig. 5.9 Modeling the association field with sub-Riemannian geodesics and exponential curves, a) the association field [26, 42]. Compare the upper-right part of the association field to the following lines: in b) we impose the end condition (blue arrows) for the SR-geodesic model in black and the end condition (red arrows) for the horizontal exponential curve model in grey; c) comparison of sub-Riemannian geodesics with exponential curves with the same (co-circularity) ending conditions; d) as in b) including other ending conditions.

5.4 The Case $d = 3$: Sub-Riemannian Geodesics in $(\mathbb{R}^3 \rtimes S^2, \Delta_3, G_1)$

In order to obtain momentum along cuspless sub-Riemannian geodesics in $(\mathbb{R}^3 \rtimes S^2, \Delta_3, G_{\beta=1})$, we apply Theorem 5.1 to the case $d = 3$ with $\mathbf{a} = \mathbf{e}_z$. We find

$$\begin{aligned}
\lambda_1(s) &= \lambda_1(0)\cosh s - \lambda_5(0)\sinh s,\\
\lambda_5(s) &= \lambda_5(0)\cosh s - \lambda_1(0)\sinh s,\\
\lambda_2(s) &= \lambda_2(0)\cosh s + \lambda_4(0)\sinh s,\\
\lambda_4(s) &= \lambda_4(0)\cosh s + \lambda_2(0)\sinh s,\\
\lambda_3(s) &= \sqrt{1-|\lambda_4(s)|^2-|\lambda_5(s)|^2},
\end{aligned} \tag{5.51}$$

and by using the horizontal part of the PMP, we now find explicit formulas for curvature and torsion of the spatial part of the sub-Riemannian geodesic:

$$\begin{aligned}
\kappa(s) &= \tfrac{\sqrt{|\lambda_4(s)|^2+|\lambda_5(s)|^2}}{\lambda_3(s)} = \tfrac{\sqrt{1-|\lambda_3(s)|^2}}{\lambda_3(s)},\\
\tau(s) &= -\tfrac{(\lambda_5(s)\lambda_2(s)+\lambda_4(s)\lambda_1(s))}{1-|\lambda_3(s)|^2} = \tfrac{W}{1-|\lambda_3(s)|^2}
\end{aligned} \tag{5.52}$$

where W denotes the Wronskian, recall Eq. (5.24), of $\lambda_5 = \frac{\kappa_1}{\sqrt{\kappa^2+1}}$ and $-\lambda_4 = \frac{\kappa_2}{\sqrt{\kappa^2+1}}$, where $\underline{\kappa} = (\kappa_1,\kappa_2) = \kappa_1\mathscr{A}_1 + \kappa_2\mathscr{A}_2$ denote the curvature components of the curvature vector-field $\ddot{\mathbf{x}} = \underline{\kappa}$ along the curve.

Consequently, we have

$$\tau(s) = W\left(1+\kappa^{-2}(s)\right)$$

whenever $\kappa(s) \neq 0$ for $s < s_{max}(\lambda(0))$ and W the constant Wronskian.

Furthermore, we see that if torsion is absent in any part of the spatial part of a sub-Riemannian geodesic it is absent everywhere, and we have

$$\gamma(s) \text{ is planar } \Leftrightarrow \tau = 0 \Leftrightarrow W = 0 \Leftrightarrow \text{ the boundary conditions are co-planar .}$$

The final equivalence, is non-trivial. For details on the proof, see [30, Cor.3.44].

Remark 5.12. The planar solutions $\mathbf{P}_{\mathbf{curve}}$ with $W = 0$ coincide with the unique two dimensional sub-Riemannian geodesics connecting the corresponding points in $\mathbb{R}^2 \rtimes S^1$ (see [8, 15]) discussed in the previous section. As a result, the set

$$\begin{aligned}
&\{\left(\mathbf{x}_{fin}, R_{\mathbf{n}_{fin}(\mathbf{x}_{fin},\theta_{fin})}\right) \mid (\mathbf{x}_{fin},\theta_{fin}) \in \mathfrak{R}_2\}\\
&\text{with } \mathbf{n}_{fin}(\mathbf{x}_{fin},\theta_{fin}) = (\sin\theta_{fin}\tfrac{x_{fin}}{\sqrt{x_{fin}^2+y_{fin}^2}}, \sin\theta_{fin}\tfrac{y_{fin}}{\sqrt{x_{fin}^2+y_{fin}^2}}, \cos\theta_{fin})^T,
\end{aligned}$$

where $\mathfrak{R}_2$ denotes the set of admissible end conditions in $SE(2)$ allowing a connection via a globally minimal sub-Riemannian geodesic in $(SE(2),\Delta_2,G_1)$, is a subset of end conditions admitting a unique globally minimizing sub-Riemannian geodesic in $(SE(3),\Delta_3,G_1)$. See Figure 5.11.

Remark 5.13. A sub-Riemannian geodesic is co-planar if $W = -\lambda_5\lambda_2 - \lambda_4\lambda_1 = 0$, i.e. if its angular momentum $(\lambda_4,\lambda_5,0) \equiv \lambda_4\omega^4 + \lambda_5\omega^5$ is orthogonal to its spatial momentum $(\lambda_1,\lambda_2,\lambda_3) \equiv \lambda_1\omega^1 + \lambda_2\omega^2 + \lambda_3\omega^3$.

Now in order to compute the exponential map $\widetilde{\mathrm{Exp}}(\lambda(0),\ell) = \gamma(\ell) = g_{fin} \in SE(3)$, one can substitute Eq. (5.52) into Eq. (5.51) while setting $s = \ell$ and then integrate

the well-known Frenet-Serret formulas for curves in $\mathbb{R}^3$. However, the last step in this procedure is somewhat cumbersome and here (again) Theorem 5.3 comes at hand.

5.4.1 Explicit Parameterizations of the Sub-Riemannian Geodesics

In order to integrate the Frenet-Serret formulas we apply Theorem 5.3 to the case $d = 3$. This provides the following explicit formulas for the sub-Riemannian geodesics, where we use the short notation $\underline{\lambda}^{(1)} = (\lambda_1, \lambda_2)$ and $\underline{\lambda}^{(2)} = (\lambda_5, \lambda_4)$ from Section 5.2.

Theorem 5.9. *Let the momentum covector be given by Eq. (5.51). Then the spatial part of the cuspless sub-Riemannian geodesics*[8] *in $(SE(3), \Delta_3, G_1)$ is given by*

$$\boldsymbol{x}(s) = \tilde{R}(0)^T (\tilde{\boldsymbol{x}}(s) - \tilde{\boldsymbol{x}}(0)) \tag{5.53}$$

where, $\tilde{R}(0)$ and $\tilde{\boldsymbol{x}}(s) := (\tilde{x}(s), \tilde{y}(s), \tilde{z}(s))$ are given in terms of $\lambda^{(1)}(0)$ and $\lambda^{(2)}(0)$ depending on several cases. For all cases, we have

$$\tilde{x}(s) = \frac{1}{\mathfrak{c}} \int_0^s \lambda_3(\tau)\, \mathrm{d}\tau. \tag{5.54}$$

For the case $\underline{\lambda}^{(1)}(0) = \boldsymbol{0}$, we have

$$\tilde{R}(0) = \begin{pmatrix} 0 & 0 & 1 \\ 0 & 1 & 0 \\ -1 & 0 & 0 \end{pmatrix} \in SO(3), \tag{5.55}$$

$$\begin{pmatrix} \tilde{y}(s) \\ \tilde{z}(s) \end{pmatrix} = \frac{-1}{\mathfrak{c}} \begin{pmatrix} \lambda_4(s) \\ \lambda_5(s) \end{pmatrix}. \tag{5.56}$$

For the case $\underline{\lambda}^{(1)}(0) \neq \boldsymbol{0}$, we have

$$\tilde{R}(0) = \frac{1}{\mathfrak{c}} \begin{pmatrix} \lambda_1(0) & \lambda_2(0) & \lambda_3(0) \\ \mathfrak{c}\frac{-\lambda_2(0)}{\|\underline{\lambda}^{(1)}(0)\|} & \mathfrak{c}\frac{\lambda_1(0)}{\|\underline{\lambda}^{(1)}(0)\|} & 0 \\ \frac{-\lambda_1(0)\lambda_3(0)}{\|\underline{\lambda}^{(1)}(0)\|} & \frac{-\lambda_2(0)\lambda_3(0)}{\|\underline{\lambda}^{(1)}(0)\|} & \|\underline{\lambda}^{(1)}(0)\| \end{pmatrix} \in SO(3). \tag{5.57}$$

For the case $W = 0$ along with $\underline{\lambda}^{(1)}(0) \neq \boldsymbol{0}$, we have

$$\begin{pmatrix} \tilde{y}(s) \\ \tilde{z}(s) \end{pmatrix} = \frac{\lambda_2(0)\lambda_4(s) - \lambda_1(0)\lambda_5(s)}{\mathfrak{c}\|\underline{\lambda}^{(1)}(0)\|} \begin{pmatrix} 0 \\ 1 \end{pmatrix}. \tag{5.58}$$

[8] which are the lifts of the stationary curves of $\mathbf{P}_{\mathbf{curve}}$ for appropriate boundary conditions and which coincide with the solutions of $\mathbf{P}_{\mathbf{mec}}$ for the same boundary conditions.

While for $W \neq \boldsymbol{0}$ along with $\underline{\lambda}^{(1)}(0) \neq \boldsymbol{0}$ and

$$A(s) = \frac{1}{\|\underline{\lambda}^{(2)}(0)\|^2 - \frac{W^2}{\mathfrak{c}^2}} \begin{pmatrix} \lambda_2(s)\lambda_4(s) - \lambda_1(s)\lambda_5(s) & -\frac{W}{\mathfrak{c}}\lambda_3(s) \\ \frac{W}{\mathfrak{c}}\lambda_3(s) & \lambda_2(s)\lambda_4(s) - \lambda_1(s)\lambda_5(s) \end{pmatrix}, \tag{5.59}$$

we have

$$\begin{pmatrix} \tilde{y}(s) \\ \tilde{z}(s) \end{pmatrix} = \frac{e^{\int_0^s A(s')\,\mathrm{d}s'}}{\mathfrak{c}^2\|\underline{\lambda}^{(1)}(0)\|} \begin{pmatrix} W\lambda_3(0) \\ \mathfrak{c}(\lambda_2(0)\lambda_4(0) - \lambda_5(0)\lambda_1(0)) \end{pmatrix}. \tag{5.60}$$

Proof. From Theorem 5.3, we have

$$\mathrm{d}(\lambda m(\gamma)^{-1}) = 0 \tag{5.61}$$

with $\lambda = (\lambda_1, \ldots, \lambda_6)$, the Lagrange multipliers which are already known by Theorem 5.1, and with matrix representation m given by Eq. (5.30). Hence, as $\gamma(0) = \mathbf{e}$, we have that $\forall s \in [0, \ell]$ the geodesic must satisfy

$$\lambda(s) = \lambda(0)m(\gamma(s)). \tag{5.62}$$

To make calculations easier, we translate and rotate the curve and solve a slightly easier equation and transform it back to the original curve. With $m(\tilde{g}) = \begin{pmatrix} \tilde{R} & \sigma_{\tilde{\mathbf{x}}}\tilde{R} \\ 0 & \tilde{R} \end{pmatrix}$, we solve the system

$$\lambda(s) = (\mathfrak{c}, 0, 0, -\frac{W}{\mathfrak{c}}, 0, 0)m(\tilde{\gamma}(s)) \tag{5.63}$$

with $\tilde{\gamma}(s) = \tilde{\gamma}(0)m(\gamma(s))$ such that

$$\lambda(0) = (\mathfrak{c}, 0, 0, -\frac{W}{\mathfrak{c}}, 0, 0)\tilde{\gamma}(0). \tag{5.64}$$

Thus after having $\tilde{\gamma}(s)$, we retrieve the geodesic by using the relation

$$\gamma(s) = \tilde{\gamma}(0)^{-1}\tilde{\gamma}(s). \tag{5.65}$$

For the most general case, assuming non-vanishing denominators throughout, we see that choosing (5.57) and

$$\tilde{\mathbf{x}}(0) := \frac{1}{\mathfrak{c}^2\sqrt{|\lambda_1(0)|^2 + |\lambda_2(0)|^2}} \begin{pmatrix} 0 \\ W\lambda_3 \\ \mathfrak{c}(\lambda_2\lambda_4 - \lambda_5\lambda_1) \end{pmatrix},$$

(5.64) is satisfied. Then solving (5.63) for $\tilde{x}$, $\tilde{y}$ and $\tilde{z}$ we obtain $\tilde{x}$ and the following system:

$$\begin{pmatrix} \dot{\tilde{y}}(s) \\ \dot{\tilde{z}}(s) \end{pmatrix} = A(s) \begin{pmatrix} \tilde{y}(s) \\ \tilde{z}(s) \end{pmatrix}.$$

Noting that $A(s)$ and $A(t)$ commute for all pairs s and t, and hence using Wilcox formula [56], we get the desired results.

Clearly, the formulas are not valid as the denominators in some of the expressions become zero. Hence we do the whole procedure keeping in mind the special cases right from the start and get the required results.

The matrix $e^{\int_0^s A(s')\mathrm{d}s'}$ can be computed explicitly, for details see [30, Cor.4.11]. One has $e^{\int_0^s A(s')\,\mathrm{d}s'} = \sqrt{\frac{\|\underline{\lambda}^{(2)}(s)\|^2 - W^2\mathfrak{c}^{-2}}{\|\underline{\lambda}^{(2)}(0)\|^2 - W^2\mathfrak{c}^{-2}}} \begin{pmatrix} \cos\phi(s) & -\sin\phi(s) \\ \sin\phi(s) & \cos\phi(s) \end{pmatrix}$, with $\phi(s) = \int_0^s \frac{W\mathfrak{c}^{-1}\lambda_3(s')}{\|\underline{\lambda}^{(2)}(s')\|^2 - W^2\mathfrak{c}^{-2}}\,\mathrm{d}s'$.

5.4.2 *Explicit Definition of the Exponential Map of* $\mathbf{P}_{\mathbf{curve}}$

In this section, we provide the explicit definition of the exponential map which maps the pair $(\lambda(0), \ell)$ to the endpoint $g_{fin} = \widetilde{\mathrm{Exp}}(\lambda(0), \ell)$ of the corresponding cusp-less sub-Riemannian geodesic in sub-Riemannian manifold $(SE(3), \Delta_3, G_1)$.

Definition 5.1. Using the arc-length parametrization and setting $t = s$ ($\Rightarrow \sigma = 1$), we consider the canonical ODE system for $\Gamma(s) = (g(s), \kappa(s), \lambda(s))$ given by

$$\begin{aligned} \dot{\Gamma}(s) &= F(\Gamma(s)) \qquad\qquad s \in [0, \ell] \\ \Gamma(0) &= (e, \kappa(0), \lambda(0)) \end{aligned}$$

with unity element $e = (\mathbf{0}, I) \in SE(3)$ and with $\kappa = (\kappa_1, \kappa_2)^T$ where $\kappa_1(0) = \frac{\lambda_5(0)}{\sqrt{1-(\lambda_4(0)^2+\lambda_5(0)^2)}}$ and $\kappa_2(0) = \frac{-\lambda_4(0)}{\sqrt{1-(\lambda_4(0)^2+\lambda_5(0)^2)}}$ where F denotes the corresponding flow field given as

$$\begin{aligned} &F\left(\begin{pmatrix} R & \sigma_{\mathbf{x}} R \\ 0 & R \end{pmatrix}, \kappa(s), \lambda(s)\right) = \\ &\left(\begin{pmatrix} RK & R\sigma_{e_z} + \sigma_x RK \\ 0 & RK \end{pmatrix}, \frac{\lambda_2\lambda_4 - \lambda_1\lambda_5}{\lambda_3^3} \begin{pmatrix} \lambda_5 \\ -\lambda_4 \end{pmatrix} - \frac{1}{\lambda_3} \begin{pmatrix} \lambda_1 \\ \lambda_2 \end{pmatrix}, \lambda \begin{pmatrix} K & \sigma_{e_z} \\ 0 & K \end{pmatrix}\right) \end{aligned} \tag{5.66}$$

where $K = \frac{1}{\lambda_3} \begin{pmatrix} 0 & 0 & \lambda_5 \\ 0 & 0 & -\lambda_4 \\ -\lambda_5 & \lambda_4 & 0 \end{pmatrix}$. and $\sigma_{\mathbf{e}_z} \in \mathbb{R}^{3\times 3}$ such that $\sigma_{\mathbf{e}_z}\mathbf{x} = \mathbf{e}_z \times \mathbf{x}$.This ODE has a unique solution

$$\Gamma(s) = \Gamma(0)e^{sF} \qquad s \in [0, \ell].$$

Recall the definition of $\mathfrak{D}$ in Eq. (5.31) (for $d = 3$). On this set, we define $\widetilde{Exp}_e : \mathfrak{D} \to SE(3)$ by

$$\widetilde{Exp}_e(\lambda(0), l) = \pi \circ e^{lF}(e, \kappa(0), \lambda(0))$$

with π being the natural projection on $SE(3)$. Note that this exponential map is different from the Lie group valued exponential map defined on the Lie algebra.

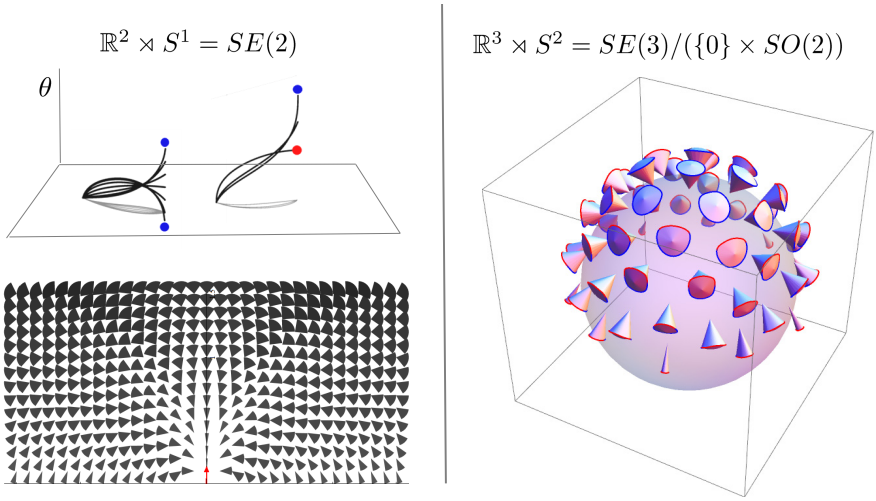

Fig. 5.10 A comparison of the possible end conditions of $\mathbf{P}_{\mathbf{curve}}$ for the two dimensional and the three dimensional cases. Right: possible tangent directions are depicted of cuspless sub-Riemannian geodesics in $(SE(3), \Delta_3, G_1)$ with initial position at the origin and the initial direction along $\mathbf{e}_z$ and the final positions at unit distance from the origin. Left: cones of possible end conditions of cuspless sub-Riemannian geodesics in $(SE(2), \Delta_2, G_1)$. According to Theorem 5.7, these cones are obtained by considering the end conditions of sub-Riemannian geodesics that either begin with a cusp point (shown in red) or end at a cusp point (shown in blue). Figure 5.11 depicts the comparison in the special case when we set the end conditions on a unit circle containing the z-axis.

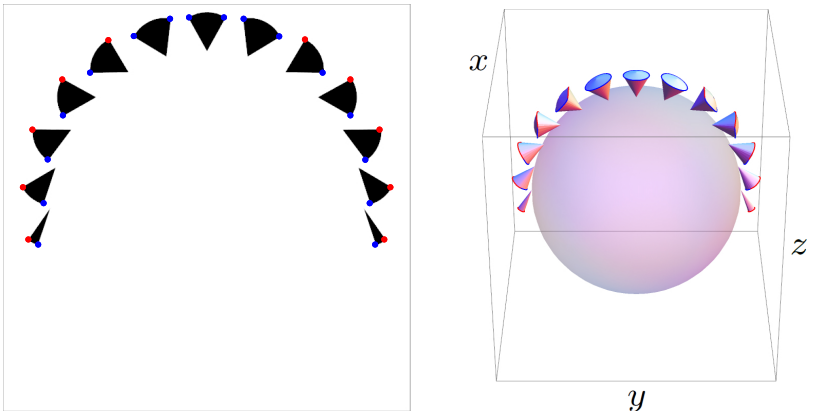

Fig. 5.11 A comparison of the cones of reachable angles by the cuspless sub-Riemannian geodesics in the two dimensional case as in [8, 15] (left) and those in the three dimensional case (right). It represents the special case in Figure 5.10, of the end conditions being on a unit circle containing the z-axis. The intersection of the cones in Figure 5.11 right with $x = 0$ coincides with the cones depicted in Figure 5.11 left.

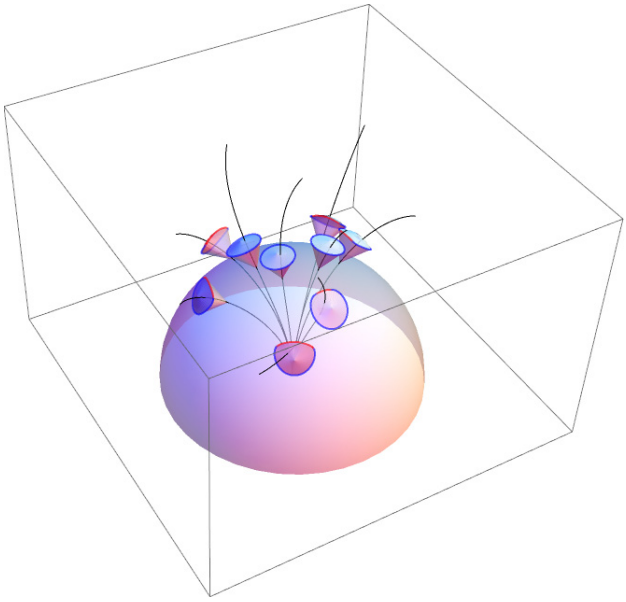

Fig. 5.12 An illustration of the spatial part of arbitrary cuspless sub-Riemannian geodesics in $(SE(3), \Delta_3, G_1)$ and the cones of reachable angles as depicted in Figures 5.10 and 5.11. The cuspless sub-Riemannian geodesics are always contained within the cones. We checked this for many more cases, which supports our Conjecture 5.2.

5.4.3 *The Range of the $\widetilde{Exp}$ Map and Cones of Reachable Angles*

There are various restrictions on the possible boundary conditions for which we can get a cuspless sub-Riemannian geodesic of problem $\mathbf{P}_{\mathbf{curve}}$, see Fig. 5.10. We present some special cases which help us to get an idea about the range of the exponential map of $\mathbf{P}_{\mathbf{curve}}$. Note that this set coincides with the set of end conditions for which $\mathbf{P}_{\mathbf{curve}}$ is expected to be well defined, as we have shown for the 2D-case (recall Theorem 5.5). The next corollary gives us the possible final positions when the final direction is anti parallel to the initial direction.

Corollary 5.3. *Let $(\boldsymbol{x}_1, \boldsymbol{n}_1)$ be the end condition of $\mathbf{P}_{\mathbf{curve}}$ with the initial condition being $(\boldsymbol{0}, \boldsymbol{e}_z)$. Then, given that $\boldsymbol{n}_1 = -\boldsymbol{e}_z$, a cuspless sub-Riemannian geodesic of problem $\mathbf{P}_{\mathbf{curve}}$ exists only for $\boldsymbol{x}_1 \cdot \boldsymbol{e}_z = 0$. Moreover, this condition is only possible for curves departing from a cusp and ending in a cusp.*

Proof. Let $\mathbf{x}$ be a cuspless sub-Riemannian geodesic of problem $\mathbf{P}_{\mathbf{curve}}$ with $\dot{\mathbf{x}}(0) = -\dot{\mathbf{x}}(\ell)$ for some $\ell \leq s_{max}$. This means that going to the tilde coordinates, we have $\tilde{\dot{\mathbf{x}}}(0) = -\tilde{\dot{\mathbf{x}}}(\ell)$, which implies $\dot{\tilde{x}}(0) = -\dot{\tilde{x}}(\ell)$. But this is possible only if $\dot{\tilde{x}}(0) = 0 = \dot{\tilde{x}}(\ell)$, which is possible only if $\|\underline{\lambda}^{(2)}(0)\| = 1$ and $\ell = s_{max}$, i.e., if the geodesic both starts and ends in cusp. □

Now we recall from Subsection 5.3.2, that in the 2D-case cuspless sub-Riemannian geodesics in $(SE(2),\Delta_2,G_1)$ are contained in the half space $x \geq 0$ and $x = 0$ can only be reached with sub-Riemannian geodesics both departing from and ending in a cusp. In the 3D-case one expects a similar result, as it is confirmed by many numerical experiments, see e.g. Figure 5.12 and Figure 5.11. However, it turns out to be hard to prove for all cases. At least we have the following formal result.

Corollary 5.4. *If a cuspless sub-Riemannian geodesic departs from a cusp, then it can never have a negative component along the z-axis. Moreover, it can meet the $z = 0$ plane at non zero time only if $s = s_{max}$ and $W = 0$.*

Proof. See [30, Lemma 4.13].

Based on our numerical experiments, we pose the following conjecture which is analogous to a result in the two dimensional case of finding cuspless sub-Riemannian geodesics in $(SE(3),\Delta_3,G_1)$ [8, 15].

Conjecture 5.2. Let the range of the exponential map defined in Definition 5.1 be denoted by $\mathfrak{R}$ and let $\mathfrak{D}$ be as defined in Definition 5.1.

- $\widetilde{Exp}_e : \mathfrak{D} \to \mathfrak{R}$ is a homeomorphism when $\mathscr{D}$ and $\mathscr{R}$ are equipped with the subspace topology.
- $\widetilde{Exp}_e : \mathring{\mathfrak{D}} \to \mathring{\mathfrak{R}}$ is a diffeomorphism. Here $\mathring{S}$ denotes the interior of the set S.

The boundary of the range is given as

$$\begin{aligned}
&\partial\mathfrak{R} = \mathscr{S}_B \cup \mathscr{S}_R \cup \mathscr{S}_L \text{ with} \qquad (5.67)\\
&\mathscr{S}_B = \{\widetilde{Exp}_e(\lambda(0), s_{max}(\lambda(0)))|\lambda(0) \in \mathscr{C}\} \text{ and}\\
&\mathscr{S}_R = \{\widetilde{Exp}_e(\lambda(0), s)|\lambda(0) \in \mathscr{C} \text{ and } \lambda_4(0)^2 + \lambda_5(0)^2 = 1 \text{ and } s > 0\}\\
&\mathscr{S}_L = \{(\mathbf{0}, R_{\mathbf{n}}) \in SE(3)|\mathbf{n} \in S^2\}.
\end{aligned}$$

This conjecture would imply that no conjugate points, recall Remark 5.4, arise within $\mathfrak{R}$ and problem $\mathbf{P_{curve}}$ (5.3) is well posed for *all* end conditions in $\mathfrak{R}$.

The proof of this conjecture would be on similar lines as in Appendix F of [15]. If the conjecture is true, we have a reasonably limited set of possible directions per given final positions for which a cuspless sub-Riemannian geodesic of problem $\mathbf{P_{curve}}$ exists. Then likewise the $d = 2$ case, we have that every end condition in $\mathfrak{R}$ can be connected with a unique minimizer of a well-posed problem $\mathbf{P_{curve}}$. Moreover, the cones determined by $\mathscr{S}_B$ and $\mathscr{S}_R$ provide the boundaries of the field of reachable cones. Figure 5.11 shows the special case of the end conditions being on a unit circle containing the z-axis. The final tangents are always contained within the cones at each position. Numerical computations indeed seem to confirm that this is the case (see Figure 5.12). The blue points on the boundary of the cones correspond to $\mathscr{S}_B$ while the red points correspond to $\mathscr{S}_R$ given in Equality (5.67).

5.5 The Case $d = 4$: Sub-Riemannian Geodesics in $(SE(4), \Delta_4, G_1)$

Let us apply the results regarding sub-Riemannian geodesics in $(SE(d), \Delta_d, G_{\beta=1})$ to the special case $d = 4$. Here we will rely on the standard matrix group representation of $SE(4)$ given by $M(g) = \begin{pmatrix} R & \mathbf{x} \\ \mathbf{0} & 1 \end{pmatrix} \in \mathbb{R}^{5\times 5}$, for all $g = (\mathbf{x}, R) \in SE(4)$. In matrix-form, the Lie-algebra elements spanning $T_e(SE(4))$ are given by

$$A_k = \mathscr{A}_k|_e \equiv \begin{pmatrix} \mathbf{0} & \mathbf{e}_k \\ \mathbf{0} & 0 \end{pmatrix}$$

for $k = 1 \ldots 4$, with $(\mathbf{e}_k)^j = \delta_k^j$, and

$$A_5 = \begin{pmatrix} 0&0&0&0&0 \\ 0&0&0&0&0 \\ 0&0&0&-1&0 \\ 0&0&1&0&0 \\ 0&0&0&0&0 \end{pmatrix}, A_6 = \begin{pmatrix} 0&0&0&0&0 \\ 0&0&0&1&0 \\ 0&0&0&0&0 \\ 0&-1&0&0&0 \\ 0&0&0&0&0 \end{pmatrix}, A_7 = \begin{pmatrix} 0&0&0&1&0 \\ 0&0&0&0&0 \\ 0&0&0&0&0 \\ -1&0&0&0&0 \\ 0&0&0&0&0 \end{pmatrix},$$

$$A_8 = \begin{pmatrix} 0&0&0&0&0 \\ 0&0&-1&0&0 \\ 0&1&0&0&0 \\ 0&0&0&0&0 \\ 0&0&0&0&0 \end{pmatrix}, A_9 = \begin{pmatrix} 0&0&1&0&0 \\ 0&0&0&0&0 \\ -1&0&0&0&0 \\ 0&0&0&0&0 \\ 0&0&0&0&0 \end{pmatrix}, A_{10} = \begin{pmatrix} 0&1&0&0&0 \\ -1&0&0&0&0 \\ 0&0&0&0&0 \\ 0&0&0&0&0 \\ 0&0&0&0&0 \end{pmatrix}.$$

The commutator table is given by

$$[A_i, A_j]_{i,j=1\ldots 10} = \begin{pmatrix} 0&0&0&0&0&0&A_4&0&A_3&A_2 \\ 0&0&0&0&0&A_4&0&-A_3&0&-A_1 \\ 0&0&0&0&-A_4&0&0&A_2&-A_1&0 \\ 0&0&0&0&A_3&-A_2&-A_1&0&0&0 \\ 0&0&A_4&-A_3&0&A_8&-A_9&-A_6&A_7&0 \\ 0&-A_4&0&A_2&-A_8&0&A_{10}&A_5&0&-A_7 \\ -A_4&0&0&A_1&A_9&-A_{10}&0&0&-A_5&A_6 \\ 0&A_3&-A_2&0&A_6&-A_5&0&0&-A_{10}&A_9 \\ -A_3&0&A_1&0&-A_7&0&A_5&A_{10}&0&-A_8 \\ -A_2&A_1&0&0&0&A_7&-A_6&A_9&A_8&0 \end{pmatrix}$$

and the PMP produces the following ODE for the momentum components:

$$\dot{\lambda}_i(t) = -\sum_{j=4}^{7}\sum_{k=1}^{7} c_{ij}^k \lambda_j(t)\lambda_k(t),$$

or more explicitly, using the fact that $\lambda_8 = \lambda_9 = \lambda_{10} = 0$ yields

$$\begin{aligned}
&\dot{\lambda}_1(t) = -\lambda_4(t)\,\lambda_7(t), && \dot{\lambda}_6(t) = -\lambda_2(t)\,\lambda_4(t),\\
&\dot{\lambda}_2(t) = -\lambda_4(t)\,\lambda_6(t), && \dot{\lambda}_7(t) = -\lambda_1(t)\,\lambda_4(t),\\
&\dot{\lambda}_3(t) = \lambda_4(t)\,\lambda_5(t), && \dot{\lambda}_8(t) = 0,\\
&\dot{\lambda}_4(t) = -\lambda_3(t)\,\lambda_5(t) + \lambda_2(t)\,\lambda_6(t) + \lambda_1(t)\,\lambda_7(t), && \dot{\lambda}_9(t) = 0,\\
&\dot{\lambda}_5(t) = \lambda_3(t)\,\lambda_4(t), && \dot{\lambda}_{10}(t) = 0.
\end{aligned}$$

Along *cuspless* sub-Riemannian geodesics, this ODE-system simplifies to

$$\begin{aligned}
&\dot{\lambda}_1(s) = -\lambda_7(s), && \dot{\lambda}_6(s) = -\lambda_2(s),\\
&\dot{\lambda}_2(s) = -\lambda_6(s), && \dot{\lambda}_7(s) = -\lambda_1(s),\\
&\dot{\lambda}_3(s) = \lambda_5(s), && \dot{\lambda}_8(s) = 0,\\
&\dot{\lambda}_4(s) = -(\lambda_4(s))^{-1}(\lambda_3(s)\,\lambda_5(s) + \lambda_2(s)\,\lambda_6(s) + \lambda_1(s)\,\lambda_7(s)), && \dot{\lambda}_9(s) = 0,\\
&\dot{\lambda}_5(s) = \lambda_3(s), && \dot{\lambda}_{10}(s) = 0,
\end{aligned}$$

which is indeed a special case of Eq. (5.21) with $d = 4$ and $\Lambda = \mathrm{diag}\{-1,-1,1\}$, whose solutions are now given by Eq. (5.25) (again with $d = 4$ and $\Lambda = \mathrm{diag}\{-1,-1,1\}$).

Now the case $d = 3$ with (cuspless) sub-Riemannian geodesics on $(SE(3),\Delta_3,G_{\beta=1})$ studied in detail in the previous section, by omitting the A_1, A_7, A_9 and A_{10} directions and relabeling the indices of the Lie-algebra elements and momentum components as follows: $(2,3,4,5,6,8) \to (1,2,3,4,5,6)$.

Acknowledgements. The authors gratefully acknowledge the Russian Foundation for Basic Research (project no. 12-01-00913-a), and the Ministry of Education and Science of Russia within the federal program "Scientific and Scientific-Pedagogical Personnel of Innovative Russia" (contract no. 8209), and the European Commission ITN-FIRST, agreement No. PITN-GA-2009-238702 and the European Research Council ("Lie Analysis", contract number Stg 553333) for financial support. The research to the results of this article has received funding from the European Research Council under the European Commityâs 7^{th} Framework Program, ERC grant agreement no.335555.

Appendix A: Derivation of the Canonical Equations for Sub-Riemannian Geodesics in $(SE(d),\Delta_d,G_1)$ Using the Pontryagin Maximum Principle

Consider the sub-Riemannian manifold $M = (SE(d),\Delta_d,G_\beta)$ given by Eq. (5.14), with $\beta = 1$. Consider geometric control problem $\mathbf{P_{mec}}$ given by Eq. (5.15).

There exists a standard PMP for $\mathbb{L}_\infty([0,T])$ controls and there exists a recently generalized PMP for $\mathbb{L}_1([0,T])$ controls [55] which in this case produces (by a reparameterization argument) the same solutions, despite the fact that $\mathbb{L}_\infty([0,T]) \subset \mathbb{L}_1([0,T])$. Here we note that $\mathbf{P_{mec}}$ is equivalent to the solutions $\gamma\colon [0,T] \to SE(d)$,

with prescribed boundary conditions $\gamma(0) = (0, I)$ and $\gamma(T) = (\mathbf{x}_1, R_{\mathbf{n}_1})$, of the control problem

$$\int_0^T L(u^d(t), \ldots, u^{2d-1}(t))\mathrm{d}t \to \quad \text{minimize (with fixed } T)$$

with

$$\dot{\gamma}(t) = \sum_{i=d}^{2d-1} u^i(t)\mathscr{A}_i|_{\gamma(t)} = \sum_{i=d}^{2d-1} \langle \omega^i|_{\gamma(t)}, \dot{\gamma}(t)\rangle \mathscr{A}_i|_{\gamma(t)}$$

where for $i = 1, 2, 3$, $u^i \in \mathbb{L}_1([0, T])$, and with Lagrangian

$$L(u^d(t), \ldots, u^{2d-1}(t)) = \sum_{i=d}^{2d-1} |u^i(t)|^2.$$

Applying the standard PMP to this problem with fixed time T, we have that there exists a Lipshitzian curve in the cotangent bundle given by $[0, T] \ni t \mapsto \mu(t) = (\gamma(t), \lambda(t)) \neq 0$ with $\lambda(t) \in T^*_{\gamma(t)}(M)$ such that

$$\begin{aligned} \dot{\mu} &= \mathbf{H}(\mu(t)) \\ H(\mu) &= \max_{u \in \mathbb{R}^d} \left(L(u^d, \ldots, u^{2d-1}) - \sum_{i=d}^{2d-1} \mu_i u^i \right) \end{aligned}$$

where $\mu = (\gamma, \lambda)$, and where the Hamiltonian is given by $H(\mu) \equiv H(\lambda) = \frac{1}{2} \sum_{i=d}^{2d-1} |\lambda_i|^2$. The Hamiltonian vector field $\mathbf{H}$ given by

$$\mathbf{H} = \sum_{i=1}^{2d-1} \alpha^i \frac{\partial}{\partial \lambda_i} + \beta^i \mathscr{A}_i \tag{5.68}$$

is such that it preserves the canonical symplectic structure

$$\sigma = \sum_{i=1}^{2d} \mathrm{d}\lambda_i \wedge \omega^i = \sum_{i=d}^{2d-1} \mathrm{d}\lambda_i \wedge \omega^i$$

and hence, we have

$$\sigma(\mathbf{H}, \cdot) = -\mathrm{d}H = -\sum_{i=d}^{2d-1} \mathscr{A}_i H \omega^i + \frac{\partial H}{\partial \lambda_i} \mathrm{d}\lambda_i. \tag{5.69}$$

From Equations (5.68), (5.69), we obtain for $i = d, \ldots, 2d-1$ that

$$\alpha^i = -\mathscr{A}_i H \text{ and } \beta^i = \frac{\partial H}{\partial \lambda_i} = \lambda_i.$$

Consequently, (noting that $\mathscr{A}_i H = 0$ for $i = 1,\dots,d$ and $i = 2d,\dots,d(d+1)/2$), we have the Hamiltonian vector field

$$\begin{aligned}\mathbf{H}(\mu) &= \sum_{i=d}^{2d-1} \beta^i \mathscr{A}_i - \sum_{i=d+1}^{2d-1}\sum_{k=1}^{2d-1}\sum_{j=d}^{2d-1} c_{i,j}^k \lambda_k \beta^j \omega^i \\ &= \sum_{i=d}^{2d-1} \lambda_i \mathscr{A}_i - \sum_{i=d+1}^{2d-1}\sum_{k=1}^{2d-1}\sum_{j=d}^{2d-1} c_{i,j}^k \lambda_k \lambda_j \omega^i\end{aligned}$$

So now let us consider the full canonical ODE in the PMP: $\dot{\mu} = \mathbf{H}(\mu)$.

Clearly, the horizontal part of PMP (where time derivatives are w.r.t. sub-Riemannian arclength t) is given as

$$\dot{\gamma} = \sum_{i=d}^{2d-1} \lambda_i \mathscr{A}_i|_\gamma \Rightarrow \lambda_i(t) = \langle \omega^i|_{\gamma(t)}, \dot{\gamma}(t)\rangle \text{ for } i = d,\dots,2d-1.$$

The vertical part of PMP gives

$$\frac{d}{dt}\sum_{i=1}^{2d-1} \lambda_i(t)\ \omega^i\big|_{\gamma(t)} = \sum_{i=1}^{2d-1} \dot{\lambda}_i(t)\ \omega^i\big|_{\gamma(t)} + \lambda_i(t)\frac{d}{dt}\ \omega^i\big|_{\gamma(t)} = -\sum_{i=d+1}^{2d-1}\sum_{k=1}^{2d-1}\sum_{j=d}^{2d-1} c_{i,j}^k \lambda_k \lambda_j\ \omega^i\big|_{\gamma(t)}$$

which is equivalent to

$$\sum_{i=1}^{2d-1} \dot{\lambda}_i\ \omega^i\big|_\gamma + \sum_{i=1}^{d} \lambda_i \left(\sum_{k=d}^{2d-1}\sum_{j=1}^{d} c_{j,k}^i \dot{\gamma}^k\ \omega^j\big|_\gamma\right) = -\sum_{i=d+1}^{2d-1}\sum_{k=1}^{2d-1}\sum_{j=d}^{2d-1} c_{i,j}^k \lambda_k \lambda_j\ \omega^i\big|_\gamma$$

and therefore using the horizontal part of PMP we obtain

$$\begin{aligned}&\sum_{i=1}^{d}\left(\dot{\lambda}_i(t) + \sum_{k=d}^{2d-1}\sum_{j=1}^{d} c_{i,k}^j \lambda_k(t)\lambda_j(t)\right)\omega^i\big|_{\gamma(t)} = 0,\\ &\sum_{i=d+1}^{2d-1}\left(\dot{\lambda}_i(t) + \sum_{j=d}^{2d-1}\sum_{k=1}^{2d-1} c_{i,j}^k \lambda_k(t)\lambda_j(t)\right)\omega^i\big|_{\gamma(t)} = 0.\end{aligned}$$

Now in the first equation above index j can as well run from 1 to $2d-1$, since if $i \le d$ and $k > d$ then for all $j > d$ we have $c_{i,k}^j = 0$. As a result we obtain

$$\dot{\lambda}_i(t) = -\sum_{j=d}^{2d-1}\sum_{k=1}^{2d-1} c_{i,j}^k \lambda_k(t)\,\lambda_j(t), \text{ for all } i \in \{1,\dots,2d-1\}.$$

References

1. Agrachev, A.A., Sachkov, Y.L.: Control Theory from the Geometric Viewpoint. Springer (2004)
2. Agrachev, A., Boscain, U., Gauthier, J.P., Rossi, F.: The intrinsic hypoelliptic Laplacian and its heat kernel on unimodular Lie groups. J. Funct. Anal. 256, 2621–2655 (2009)
3. van Almsick, M.: Context Models of Lines and Contours, Eindhoven University of Technology. Department of Biomedical Engineering (2007), http://alexandria.tue.nl/extra2/200711652.pdf
4. Ardentov, A., Sachkov, Y.: Solution of Euler's elastic problem. Avtomatika i Telemekhanika (4), 78–88 (2009), English translation in Automation and remote control
5. Barbieri, D., Citti, G., Sanguinetti, G., Sarti, A.: An uncertainty principle underlying the functional architecture of V1. Journal of Physiology Paris 106(5-6), 183–193 (2012)
6. Ben-Yosef, G., Ben-Shahar, O.: A Tangent Bundle Theory for Visual Curve Completion. PAMI 34(7), 1263–1280 (2012)
7. Boscain, U., Charlot, G., Rossi, F.: Existence of planar curves minimizing length and curvature. Proceedings of the Steklov Institute of Mathematics 270(1), 43–56 (2010)
8. Boscain, U., Duits, R., Rossi, F., Sachkov, Y.: Curve cuspless reconstruction via sub-Riemannian geometry. SIAM (2013), http://bmia.bmt.tue.nl/people/RDuits/1203.3089v2.pdf (submitted)
9. Bruckstein, A., Holt, R., Netravali, A.: Discrete elastica. Appl. Anal. (78), 453–485 (2001)
10. Bryant, R., Griffiths, P.: Reduction for constrained variational problems and $(1/2)\int \kappa^2 ds$. American Journal of Mathematics 108(3), 525–570 (1986)
11. Bryant, R.L., Chern, S.S., Gardner, R.B., Goldschmidt, H.L., Griffiths, P.A.: Exterior differential systems. In: Mathematical Sciences Research Institute Publications. Springer (1991)
12. Chan, T.F., Kang, S.-H., Shen, J.: Euler's elastica and curvature based inpaintings. SIAM J. Appl. Math. (63), 564–594 (2002)
13. Citti, G., Sarti, A.: A cortical based model of perceptional completion in the roto-translation space. Journal of Mathematical Imaging and Vision 24(3), 307–326 (2006)
14. Dela Haije, T.C.J., Duits, R., Tax, C.: Sharpening fibers in diffusion weighted MRI via erosion. In: Visualization and Processing of Tensors and Higher Order Descriptors for Multi-Valued Data (2012), www.bmia.bmt.tue.nl/people/RDuits/DDT.pdf, Accepted for publication, bookchapter in Visualization and Processing of Tensors and Higher Order Descriptors for Multi-Valued Data. Dagstuhl Seminar 11501
15. Duits, R., Boscain, U., Rossi, F., Sachkov, Y.: Association felds via cuspless sub-Riemannian geodesics in $SE(2)$. Journal of Mathematical Imaging and Vision, 1–32 (2013), http://bmia.bmt.tue.nl/people/RDuits/cusp.pdf (submitted)
16. Duits, R., Dela Haije, T.C.J., Creusen, E.J., Ghosh, A.: Morphological and Linear scale Spaces for Fiber Enhancement in DW-MRI. Journal of Mathematical Imaging and Vision 46(3), 326–368 (2013)
17. Duits, R., Franken, E.M.: Line Enhancement and Completion via Left-invariant Scale Spaces on SE(2). In: Tai, X.-C., Morken, K., Lysaker, M., Lie, K.-A. (eds.) SSVM 2009. LNCS, vol. 5567, pp. 795–807. Springer, Heidelberg (2009)
18. Duits, R., Franken, E.M.: Left-invariant Diffusions on the Space of Positions and Orientations and their Application to Crossing-preserving Smoothing of HARDI images. IJCV 92(3), 231–264 (2011)

19. Duits, R., Franken, E.M.: Left-invariant parabolic evolution equations on SE(2) and contour enhancement via invertible orientation scores, part I: Linear left-invariant diffusion equations on SE(2). Quarterly on Applied Mathematics 68(2), 255–292 (2010)
20. Duits, R., Franken, E.M.: Left-invariant parabolic evolution equations on SE(2) and contour enhancement via invertible orientation scores, part II: Nonlinear left-invariant diffusion equations on invertible orientation scores. Quarterly on Applied Mathematics 68(2), 293–331 (2010)
21. Duits, R., van Almsick, M.: The explicit solutions of linear left-invariant second order stochastic evolution equations on the 2D Euclidean motion group. Quart. Appl. Math. 66, 27–67 (2008)
22. Duits, R., Franken, E.M.: Left-invariant Stochastic Evolution Equations on $SE(2)$ and its Applications to Contour Enhancement and Contour Completion via Invertible Orientation Scores. arXiv: 0711.0951v4, Also available as CASA report nr.35. Eindhoven University of Technology (2007), www.win.tue.nl/casa/research/casareports/2007.html
23. Duits, R., Dela Haije, T.C.J., Creusen, E.J., Ghosh, A.: Morphological and Linear scale Spaces for Fiber Enhancement in DW-MRI. Journal of Mathematical Imaging and Vision 46(3), 326–368 (2013)
24. Euler, L.: Methodus inveniedi lineas curvas maximi minimive proprietate gaudentes, sive solutio problematis isoperimitrici latissimo sensu accepti, Lausanne, Geneva (1744)
25. Ermentrout, G.B., Cowan, J.D.: A mathematical theory of visual hallucinations. Kybernetic 34, 137–150 (1979)
26. Field, D.J., Hayes, A., Hess, R.F.: Contour integration by the human visual system:evidence for a local "association field". Vision Res. 33(2), 253–278 (1993)
27. Franken, E., Duits, R.: Crossing-Preserving Coherence-Enhancing Diffusion on Invertible Orienattion Scores. IJCV 85(3), 253–278 (2009)
28. Franken, E.M.: Enhancement of Crossing Elongated Structures in Images. Ph.D. thesis, Eindhoven University of Technology, Eindhoven (2008), http://www.bmi2.bmt.tue.nl/Image-Analysis/People/EFranken/PhDThesisErikFranken.pdf
29. Frégnac, Y., Shulz, D.: Activity-dependent regulation of receptive field properties of cat area 17 by supervised Hebbain learning. J. Neurobiol. 41(1), 69–82 (1999)
30. Ghosh, A., Duits, R., Dela Haije, T.C.J.: On the Cuspless Sub-Riemannian Geodesics in $\mathbb{R}^3 \rtimes S^2$. submitted to JDCS (2013), www.bmia.bmt.tue.nl/people/RDuits/GhoshDuitsDelaHaije.pdf
31. Grossberg, S., Mingolla, E.: Neural dynamics of form perception: boundary completion, illusory figures and neon color spreading. Psych. Rev. 92, 173–211 (1985)
32. Hladky, R.K., Pauls, S.D.: Minimal Surfaces in the Roto-Translation Group with Applications to a Neuro-Biological Image Completion Model. J. Math. Imaging Vis. 36, 1–27 (2010)
33. Horn, B.K.P.: The curves of least energy. ACM Trans. Math. Software 9 (4), 441–460 (1983)
34. Georges, S., Series, P., Fregnac, Y., Lorenceau, J.: Orientation-dependent modulation of apparent speed: psychophysical evidence. Vision Res. 42, 2557–2572 (2002)
35. Mashtakov, A., Ardentov, A., Sachkov, Y.: Parallel Algorithm and Software for Image Inpainting via Sub-Riemannian Minimizers on the Group of Rototranslations. Numerical Methods: Theory and Applications 6(1), 95–115 (2013)
36. Medioni, G., Lee, M.-S., Tang, C.-K.: A computational framework for segmentation and grouping. Elsevier Science (2000)

37. Moiseev, I., Sachkov, Y.L.: Maxwell strata in sub-Riemannian problem on the group of motions of a plane. ESAIM: COCV 16(2), 380–399 (2010)
38. Mumford, D.: Elastica and computer vision. In: Algebraic Geometry and Its Applications, pp. 491–506. Springer (1994)
39. Parent, P., Zucker, S.W.: Trace interference, curvature consistency, and curve detection. IEEE Trans. Pattern Anal. Math. Intell. II 8, 823–939 (1989)
40. Petitot, J.: Vers une Neuro-géomètrie. Fibrations corticales, structures de contact et contours subjectifs modaux. Math. Inform. Sci. Humaines (145), 5–101 (1999)
41. Petitot, J.: Neurogéomètrie de la vision - Modèles mathématiques et physiques des architechtures fonctionnelles. Les Éditions de l'École Polytechnique (2008)
42. Petitot, J.: The neurogeometry of pinwheels as a sub-Riemannian contact structure. Journal of Physiology - Paris 97, 265–309 (2003)
43. Pontryagin, L.S., Boltyansij, V.G., Gamkrelidze, R.V., Mishchenko, E.F.: The Mathematical Theory of Optimal Processes. Pergamon Press, Oxford (1964)
44. Sachkov, Y.: Maxwell strata in the Euler elastic problem. J. Dyn. Control Syst. 14(2), 169–234 (2008)
45. Sachkov, Y.: Conjugate and cut time in the sub-Riemannian problem on the group of motions of a plane. ESAIM: COCV 16(4), 1018–1039 (2010)
46. Sachkov, Y.: Cut locus and optimal synthesis in the sub-Riemannian problem on the group of motions of a plane. ESAIM: COCV 17(2), 293–321 (2011)
47. Sanguinetti, G., Citti, G., Sarti, A.: Image completion using a diffusion driven mean curvature flow in a sub-Riemannian space. In: Int. Conf. on Computer Vision Theory and Applications (VISAPP 2008), Funchal (2008)
48. Sanguinetti, G., Citti, G., Sarti, A.: A model of natural image edge co-occurance in the rototranslation group. Journal of Vision 10(14), 1–16 (2010)
49. Sarti, A., Citti, G.: A cortical based model of perceptual completion in the Roto-Translation space. In: Proceeding of the Workshop on Second Order Subelliptic Equations and Applications, Cortona (June 2003)
50. MomayyezSiahkal, P., Sidiqqi, K.: 3D Stochastic Completion Fields for Mapping Connectivity in Diffusion MRI. IEEE PAMI 35(4) (2013)
51. Tai, X.-C., Hahn, J., Chung, G.S.: A fast algorithm for Euler's elastica model using augmented Lagrangian method. SIAM J. Imaging Sciences 4(1), 313–344 (2011)
52. Hahn, J., Chung, G.J., Wang, Y., Tai, X.-C.: Fast algorithms for *p*-elastica energy with the application to image inpainting and curve reconstruction. In: Bruckstein, A.M., ter Haar Romeny, B.M., Bronstein, A.M., Bronstein, M.M. (eds.) SSVM 2011. LNCS, vol. 6667, pp. 169–182. Springer, Heidelberg (2012)
53. Thornber, K.K., Williams, L.R.: Characterizing the Distribution of Completion Shapes with Corners Using a Mixture of Random Processes. Pattern Recognition 33, 543–553 (2000)
54. Ullman, S.: Filling in the gaps: the shape of subjective contours and a model for their generation. Biological Cybernetics 25, 1–6 (1976)
55. Vinter, R.: Optimal Control. Birkhauser (2010)
56. Wilcox, R.M.: Exponential operators and parameter differentiation in quantum physiscs. Journal of Mathematical Physics (1966)
57. Wittich, O.: An explicit local uniform bound on Brownian bridges. Statistics and Probability Letters 73(1), 51–56 (2005)
58. Zucker, S.W., David, C., Dobbins, A., Iverson, L.: The organization of curve detection: coarse tangent fields and fine spline covering. In: Proc. of the 2nd Int. Conf. on Computer Vision, pp. 568–577. IEEE, New York (1988)